J|A|C|S
ARTICLES
Published on Web 12/04/2004

Dioxygen Activation at a Single Copper Site: Structure, Bonding, and Mechanism of Formation of 1:1 Cu−O_2 Adducts

Nermeen W. Aboelella,[†] Sergey V. Kryatov,[‡] Benjamin F. Gherman,[†] William W. Brennessel,[†] Victor G. Young, Jr.,[†] Ritimukta Sarangi,[§] Elena V. Rybak-Akimova,[‡] Keith O. Hodgson,[§,¶] Britt Hedman,[¶] Edward I. Solomon,[§] Christopher J. Cramer,[†] and William B. Tolman*[,†]

Contribution from the Department of Chemistry, Center for Metals in Biocatalysis, and Supercomputer Institute, University of Minnesota, 207 Pleasant Street SE, Minneapolis, Minnesota 55455, Department of Chemistry, Tufts University, 62 Talbot Avenue, Medford, Massachusetts, 02155, Department of Chemistry, Stanford University, Stanford, California 94305, and Stanford Synchrotron Radiation Laboratory, Stanford University, Stanford, California 94305

Received July 19, 2004; Revised Manuscript Received October 3, 2004; E-mail: tolman@chem.umn.edu

Abstract: To evaluate the fundamental process of O_2 activation at a single copper site that occurs in biological and catalytic systems, a detailed study of O_2 binding to Cu(I) complexes of β-diketiminate ligands L (L^1 = backbone Me; L^2 = backbone *t*Bu) by X-ray crystallography, X-ray absorption spectroscopy (XAS), cryogenic stopped-flow kinetics, and theoretical calculations was performed. Using synchrotron radiation, an X-ray diffraction data set for L^2CuO_2 was acquired, which led to structural parameters in close agreement to theoretical predictions. Significant Cu(III)−peroxo character for the complex was corroborated by XAS. On the basis of stopped-flow kinetics data and theoretical calculations for the oxygenation of L^1Cu(RCN) (R = alkyl, aryl) in THF and THF/RCN mixtures between 193 and 233 K, a dual pathway mechanism is proposed involving (a) rate-determining solvolysis of RCN by THF followed by rapid oxygenation of L^1Cu(THF) and (b) direct, bimolecular oxygenation of L^1Cu(RCN) via an associative process.

Introduction

A critical function of copper centers in enzymes[1,2] and other catalysts[3] is to bind and/or activate dioxygen. In particular, O_2 activation by monocopper active sites is a central part of catalytic cycles traversed by enzymes involved in diverse metabolic processes.[4] Notable examples are dopamine β-monooxygenase (DβM)[2,5] and peptidylglycine α-hydroxylating monooxygenase (PHM),[2,6] which hydroxylate aliphatic C−H bonds of their respective substrates, dopamine or peptide hormones, to yield the neurotransmitter norepinephrine (DβM) or, after subsequent chemistry, fully bioactive C-terminal amidated peptides (PHM). Extensive similarities between these enzymes implicate analogous active site structures and catalytic mechanisms. X-ray crystallographic[6,7] and EXAFS[8] data for PHM have revealed two copper sites, one with three His ligands (Cu_H) and the other with two His and 1 Met (Cu_M) provided by the protein. Kinetic data support a mechanism for substrate attack by DβM and PHM that involves abstraction of an H-atom with quantum mechanical tunneling.[9] While there appears to be consensus that a Cu−O_2 intermediate is involved in this process, the nature of the intermediate(s) and the pathways for its(their) formation and subsequent reactions are not known. Recent kinetic,[9e] theoretical,[10] and X-ray crystallographic[7c] results suggest that a Cu(II)−O_2^- moiety at Cu_M is responsible for the H-atom abstraction. Many aspects of the properties of this species remain obscure, however, and the possible role of alternative intermediates continues to be debated (e.g., Cu(II)−OOH).[11] Similar Cu−O_2 species have been suggested as intermediates in H_2O_2 production by amine

[†] University of Minnesota.
[‡] Tufts University.
[§] Department of Chemistry, Stanford University.
[¶] Stanford Synchrotron Radiation Laboratory, Stanford University.

(1) Solomon, E. I.; Chen, P.; Metz, M.; Lee, S.-K.; Palmer, A. E. *Angew. Chem., Int. Ed.* **2001**, *40*, 4570.
(2) Klinman, J. P. *Chem. Rev.* **1996**, *96*, 2541.
(3) For a recent example, see: Markó, I. E.; Gautier, A.; Dumeunier, R.; Doda, K.; Philippart, F.; Brown, S. M.; Urch, C. J. *Angew. Chem., Int. Ed.* **2004**, *43*, 1588.
(4) Halcrow, M. A. In *Comprehensive Coordination Chemistry II*; McCleverty, J. A., Meyer, T. J., Eds.; Elsevier: Amsterdam, 2004; Vol. 8, pp 395−436.
(5) Stewart, L. C.; Klinman, J. P. *Annu. Rev. Biochem.* **1988**, *57*, 551.
(6) Prigge, S. T.; Mains, R. E.; Eipper, B. A.; Amzel, L. M. *Cell. Mol. Life Sci.* **2000**, *57*, 1236.
(7) Prigge, S. T.; Kolhekar, A. S.; Eipper, B. A.; Mains, R. E.; Amzel, L. M. *Science* **1997**, *278*, 1300. (b) Prigge, S. T.; Kolhekar, A. S.; Eipper, B. A.; Mains, R. E.; Amzel, L. M. *Nat. Struct. Biol.* **1999**, *6*, 976. (c) Prigge, S. T.; Eipper, B. A.; Mains, R. E.; Amzel, L. M. *Science* **2004**, *304*, 864.
(8) Boswell, J. S.; Reddy, B. J.; Kulathila, R.; Merkler, D.; Blackburn, N. J. *Biochemistry* **1996**, *35*, 12241. (b) Blackburn, N. J.; Rhames, F. C.; Ralle, M.; Jaron, S. *J. Biol. Inorg. Chem.* **2000**, *5*, 341. (c) Jaron, S.; Blackburn, N. J. *Biochemistry* **2001**, *40*, 6867. (d) Rhames, F. C.; Murthy, N. N.; Karlin, K. D.; Blackburn, N. J. *J. Biol. Inorg. Chem.* **2001**, *6*, 567. (e) Jaron, S.; Mains, R. E.; Eipper, B. A.; Blackburn, N. J. *Biochemistry* **2002**, *41*, 13274.
(9) Tian, G.; Berry, J. A.; Klinman, J. P. *Biochemistry* **1994**, *33*, 226. (b) Francisco, W. A.; Merkler, D. J.; Blackburn, N. J.; Klinman, J. P. *Biochemistry* **1998**, *37*, 8244. (c) Francisco, W. A.; Knapp, M. J.; Blackburn, N. J.; Klinman, J. P. *J. Am. Chem. Soc.* **2002**, *124*, 8194. (d) Francisco, W. A.; Blackburn, N. J.; Klinman, J. P. *Biochemistry* **2003**, *42*, 1813. (e) Evans, J. P.; Ahn, K.; Klinman, J. P. *J. Biol. Chem.* **2003**, *278*, 49691.
(10) Chen, P.; Solomon, E. I. *J. Am. Chem. Soc.* **2004**, *126*, 4991.
(11) Chen, P.; Bell, J.; Eipper, B. A.; Solomon, E. I. *Biochemistry* **2004**, *43*, 5735.

 10.1021/ja045678j CCC: $27.50

oxidases (AOs) and galactose oxidase (GAO),[12−14] as well as in the self-processing biogenesis of their respective cofactors (topaquinone and S−Cys-modified tyrosine).[15] However, direct structural or spectroscopic information is not available for any such species in AO or GAO, with the exception of X-ray structural evidence for product H_2O_2 near the Cu site in *Escherichia coli* AO.[16]

Significant insights into dioxygen activation by copper proteins have been obtained through synthetic modeling studies, with peroxo- and bis(μ-oxo)dicopper complexes having been especially thoroughly examined.[17] Detailed understanding of monocopper−dioxygen species is less developed, in part because in reactions of Cu(I) complexes with O_2, 1:1 Cu−O_2 intermediates are often no more than transient species that are rapidly trapped by a second Cu(I) ion to yield relatively stable dicopper complexes.[4,17b] Thus, only a few examples of isolable and well-defined synthetic monocopper−dioxygen species have been reported (Table S1 in the Supporting Information). A side-on (η^2) Cu−O_2 complex supported by a hindered tris(pyrazolyl)-hydroborate (Tp) ligand has been characterized by X-ray crystallography[18] and identified (along with an analog) as a Cu(II)−O_2^- species on the basis of spectroscopy and theory.[19] An end-on (η^1) complex has been identified by FTIR spectroscopy and shown to evolve H_2O_2 upon protonation.[20] Kinetic, UV−vis, and resonance Raman evidence for a stable Cu(II)−O_2^- complex of a tetradentate N_3O donor ligand also have been presented;[21] similar data have appeared for analogous yet less thermodynamically stable examples.[22] Finally, Cu(II)−OOR (R = acyl, alkyl, or H) complexes have been isolated that are relevant in the current context, although they are not obtained from reactions of Cu(I) complexes with O_2.[4,23]

Extensive kinetics studies of the oxygenation of Cu(I) complexes have provided some benchmark activation and thermodynamic parameters for 1:1 adduct formation, although the level of mechanistic detail available is limited.[17b,24−26] Recently, the importance of the solvent ligand (S) in (TMPA)Cu(I) complexes (TMPA = tris(pyridylmethyl)amine) on the rate of oxygenation has been defined, wherein for S = THF, faster reactions and accentuated supporting ligand electronic influences are observed relative to those when S = RCN.[27,28] Activation parameters for these and other related systems[22b] have been interpreted to indicate dissociative or associative processes for the oxygenation process, depending on the nature of S or the supporting ligand L. Notwithstanding these advances, there is a general lack of knowledge of the elementary reaction steps involved in the displacement of S from Cu(I) by O_2 and of the structure(s) of the key transition state(s) and/or intermediates involved in oxygenations that yield well-defined 1:1 Cu−O_2 adducts.

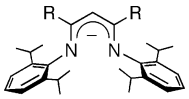

L^1 (R = Me)
L^2 (R = tBu)

In recent explorations of the O_2 chemistry of Cu(I) complexes of β-diketiminate ligands, we found that bis(μ-oxo)dicopper complex formation[29] could be inhibited by using the sterically hindered ligands L^1 and L^2.[30,31] Oxygenation of LCu(MeCN) (L = L^1 or L^2) at low temperature yielded stable η^2 1:1 Cu−O_2 adducts that were characterized by NMR, UV−vis, EPR, and resonance Raman spectroscopy, DFT calculations, and a preliminary X-ray crystal structure for L = L^2 (Table S1 in the Supporting Information). Notably, low values for the O−O stretching frequency (e.g., for L = L^2, $\nu(^{16}O_2) = 961$ cm^{-1} and $\Delta\nu(^{18}O_2) = 49$ cm^{-1}) suggested significant contribution of a Cu(III)−O_2^{2-} resonance form. This conclusion was corroborated by the relatively long O−O distance calculated (1.376 Å) and observed by crystallography (1.44 Å),[31,32] although the reliability of the latter was mitigated by the relatively poor quality of the X-ray structural data coupled with extreme disorder of the molecule in the crystal.

Herein, we report revised X-ray crystallographic results for L^2CuO_2 based on a better quality data set acquired using a synchrotron radiation source. Further insight into the geometry

(12) Halcrow, M.; Phillips, S.; Knowles, P. In *Subcellular Biochemistry, Vol. 35: Enzyme-Catalyzed Electron and Radical Transfer*; Holzenburg, A., Scrutton, N. S., Eds.; Plenum: New York, 2000; pp 183−231.
(13) Klinman, J. P. *J. Biol. Inorg. Chem.* **2001**, *6*, 1.
(14) Whittaker, J. W. *Chem. Rev.* **2003**, *103*, 2347.
(15) Dooley, D. M. *J. Biol. Inorg. Chem.* **1999**, *4*, 1. (b) Rogers, M. S.; Baron, A. J.; McPherson, M. J.; Knowles, P. F.; Dooley, D. M. *J. Am. Chem. Soc.* **2000**, *122*, 990. (c) Firbank, S. J.; Rogers, M. S.; Wilmot, C. M.; Dooley, D. M.; Halcrow, M. A.; Knowles, P. F.; McPherson, M. J. *Proc. Natl. Acad. Sci. U.S.A.* **2001**, *98*, 12932.
(16) Wilmot, C. M.; Hajdu, J.; Mcpherson, M. J.; Knowles, P. F.; Phillips, S. E. V. *Science* **1999**, *286*, 1724.
(17) For selected recent reviews, see: (a) Mirica, L. M.; Ottensaelder, X.; Stack, T. D. P. *Chem. Rev.* **2004**, *104*, 1013. (b) Lewis, E. A.; Tolman, W. B. *Chem. Rev.* **2004**, *104*, 1047. (c) Itoh, S. In *Comprehensive Coordination Chemistry II*; McCleverty, J. A., Meyer, T. J., Eds.; Elsevier: Amsterdam, 2004; Vol. 8, pp 369−393. (d) Stack, T. D. P. *Dalton Trans.* **2003**, 1881. (e) Que, L., Jr.; Tolman, W. B. *Angew. Chem., Int. Ed.* **2002**, *41*, 1114. (f) Kopf, M.-A.; Karlin, K. D. In *Biomimetic Oxidations Catalyzed by Transition Metal Complexes*; Meunier, B., Ed.; Imperial College Press: London, 2000; pp 309−362.
(18) Fujisawa, K.; Tanaka, M.; Moro-oka, Y.; Kitajima, N. *J. Am. Chem. Soc.* **1994**, *116*, 12079.
(19) Chen, P.; Root, D. E.; Campochiaro, C.; Fujisawa, K.; Solomon, E. I. *J. Am. Chem. Soc.* **2003**, *125*, 466.
(20) Chaudhuri, P.; Hess, M.; Weyhermüller, T.; Wieghardt, K. *Angew. Chem., Int. Ed.* **1999**, *38*, 1095.
(21) Jazdzewski, B. A.; Reynolds, A. M.; Holland, P. L.; Young, V. G., Jr.; Kaderli, S.; Zuberbühler, A. D.; Tolman, W. B. *J. Biol. Inorg. Chem.* **2003**, *8*, 381.
(22) Komiyama, K.; Furutachi, H.; Nagatomo, S.; Hashimoto, A.; Hayashi, H.; Fujinami, S.; Suzuki, M.; Kitagawa, T. *Bull. Chem. Soc. Jpn.* **2004**, *77*, 59. (b) Weitzer, M.; Schindler, S.; Brehm, G.; Schneider, S.; Hörmann, E.; Jung, B.; Kaderli, S.; Zuberbühler, A. D. *Inorg. Chem.* **2003**, *42*, 1800.
(23) Fujisawa, K.; Kobayashi, T.; Kitajima, N.; Moro-oka, Y. *J. Am. Chem. Soc.* **1996**, *118*, 1. (b) Kitajima, N.; Katayama, T.; Fujisawa, K.; Iwata, Y.; Moro-oka, Y. *J. Am. Chem. Soc.* **1993**, *115*, 7872. (c) Sanyal, I.; Ghosh, P.; Karlin, K. *Inorg. Chem.* **1995**, *34*, 3050. (d) Chen, P.; Fujisawa, K.; Solomon, E. I. *J. Am. Chem. Soc.* **2000**, *122*, 10177. (e) Wada, A.; Harata, M.; Hasegawa, K.; Jitsukawa, K.; Masuda, H.; Mukai, M.; Kitagawa, T.; Einaga, H. *Angew. Chem., Int. Ed.* **1998**, *37*, 798. (f) Kodera, M.; Kita, T.; Miura, I.; Nakayama, N.; Kawata, T.; Kano, K.; Hirota, S. *J. Am. Chem. Soc.* **2001**, *123*, 7715. (g) Yamaguchi, S.; Nagatomo, S.; Kitagawa, T.; Funahashi, Y.; Ozawa, T.; Jitsukawa, K.; Masuda, H. *Inorg. Chem.* **2003**, *42*, 6968. (h) Fujii, T.; Naito, A.; Yamaguchi, S.; Wada, A.; Funahashi, Y.; Jitsukawa, K.; Nagatomo, S.; Kitagawa, T.; Masuda, H. *Chem. Commun.* **2003**, 2700.
(24) Karlin, K. D.; Tolman, W. B.; Kaderli, S.; Zuberbühler, A. D. *J. Mol. Catal. A* **1997**, *117*, 215.
(25) Schindler, S. *Eur. J. Inorg. Chem.* **2000**, 2311.
(26) For a previous report on the kinetics of the formation of a 1:1 Cu/O_2 adduct supported by BQPA (a bis(quinolyl) derivative of TMPA) that has been revised (2:1 species are involved instead), see: (a) Karlin, K. D.; Wei, N.; Jung, B.; Kaderli, S.; Niklaus, P.; Zuberbühler, A. D. *J. Am. Chem. Soc.* **1993**, *115*, 9506. (b) Wick, P. K.; Karlin, K. D.; Suzuki, M.; Zuberbühler, A. D. *Micron* **2004**, *35*, 137.
(27) Zhang, C. X.; Kaderli, S.; Costas, M.; Kim, E.; Neuhold, Y.-M.; Karlin, K. D.; Zuberbühler, A. D. *Inorg. Chem.* **2003**, *42*, 1807.
(28) Fry, H. C.; Scaltrito, D. V.; Karlin, K. D.; Meyer, G. J. *J. Am. Chem. Soc.* **2003**, *125*, 11866.
(29) Spencer, D. J. E.; Reynolds, A. M.; Holland, P. L.; Jazdzewski, B. A.; Duboc-Toia, C.; Pape, L. L.; Yokota, S.; Tachi, Y.; Itoh, S.; Tolman, W. B. *Inorg. Chem.* **2002**, *41*, 6307.
(30) Spencer, D. J. E.; Aboelella, N. W.; Reynolds, A. M.; Holland, P. L.; Tolman, W. B. *J. Am. Chem. Soc.* **2002**, *124*, 2108.
(31) Aboelella, N. W.; Lewis, E. A.; Reynolds, A. M.; Brennessel, W. W.; Cramer, C. J.; Tolman, W. B. *J. Am. Chem. Soc.* **2002**, *124*, 10660.

and electronic structure of the 1:1 Cu−O_2 adduct has been provided by X-ray absorption spectroscopy. In addition, we have completed a cryogenic stopped-flow kinetic study of the formation of L^1CuO_2 from the reaction of O_2 with L^1Cu(NCR) complexes and have analyzed the oxygenation reaction pathway(s) by theoretical methods. On the basis of the combined and cross-validated experimental and theoretical results, a detailed mechanism for the oxygenation reaction is proposed.

Experimental Section

General Considerations. All reagents were obtained from commercial sources and used as received unless stated otherwise. The solvents, tetrahydrofuran (THF), heptane, and pentane, were distilled from Na/benzophenone or passed through solvent purification columns (Glass Contour, Laguna, CA). Acetonitrile (CH_3CN) was distilled from calcium hydride. Acetone was distilled from anhydrous calcium sulfate. All metal complexes were prepared and stored in a vacuum atmospheres inert atmosphere glovebox under a dry nitrogen atmosphere or were manipulated using standard Schlenk techniques. The Cu(I) compounds, LCu(MeCN) (L = L^1 or L^2), and their O_2 adducts, $LCuO_2$, were prepared as reported previously.[29−31] NMR spectra were recorded on a Varian VI-300 or VXR-300 spectrometer. Chemical shifts (δ) for ^{1}H or ^{13}C NMR spectra were referenced to residual protium in the deuterated solvent. UV−vis spectra were recorded on an HP8453 (190−1100 nm) diode array spectrophotometer. Low-temperature spectra were acquired using a custom-manufactured vacuum dewar equipped with quartz windows, with low temperatures achieved with the use of a low-temperature MeOH bath circulator.

[(L^1Cu)$_2$(*p*-NC-C_6H_4-CN)]. A solution of L^1Cu(MeCN) (0.121 g, 0.232 mmol) in THF (2 mL) was added to a stirring solution of 1,4-dicyanobenzene (0.015 g, 0.117 mmol) in THF (2 mL). A deep purple color developed upon complete addition of L^1Cu(MeCN). After the mixture was stirred for 30 min, solvent was removed under reduced pressure, and the resulting residue was washed with 2−3 mL of heptane, collected by filtration, and then dried in vacuo to yield a purple solid (67 mg, 53%). X-ray quality crystals were obtained by cooling a concentrated pentane solution to 253 K. ^{1}H NMR (300 MHz, C_6D_6): δ 7.06−7.19 (m, 6H), 6.03 (br s, 2H), 5.00 (s, 1H), 3.54 (heptet, J = 6.9 Hz, 4H), 1.85 (s, 6H), 1.39 (d, J = 6.9 Hz, 12H), 1.27 (d, J = 6.9 Hz, 12H). ^{13}C{^{1}H} NMR (75 MHz, C_6D_6): δ 163.63, 148.94, 141.04, 131.92, 124.04, 123.73, 116.78, 115.25, 94.00, 28.56, 24.91, 23.86, 23.75. UV−vis (THF) [λ_{max}, nm (ϵ, M^{-1} cm^{-1})]: 281 (31100), 349 (35700), 525 (5300). Anal. Calcd for $C_{66}H_{86}N_6Cu_2$: C, 72.69; H, 7.95; N, 7.71. Found: C, 72.05; H, 8.45; N, 7.76.

L^1Cu(*p*-NC-C_6H_4-OMe). A solution of 4-methoxybenzonitrile (0.031 g, 0.233 mmol) in THF (2 mL) was added to a stirring solution of L^1Cu(MeCN) (0.096 g, 0.184 mmol) in THF (2 mL). After the mixture was stirred for 45 min, solvent was removed under reduced pressure to yield a yellow residue. The residue was extracted with approximately 10 mL of pentane, and the extract was filtered through Celite. The volume of the filtrate was reduced to approximately 1 mL and placed in a 253 K freezer. After several days, large orange crystals of the product formed, which were isolated, washed with a minimal amount of cold pentane, and dried in vacuo (0.071 g, 63%). ^{1}H NMR (300 MHz, C_6D_6): δ 7.10−7.23 (m, 6H), 6.52 (m, 2H), 6.15 (m, 2H), 5.03 (s, 1H), 3.63 (heptet, J = 6.9 Hz, 4H), 2.90 (s, 3H), 1.89 (s, 6H), 1.47 (d, J = 6.9 Hz, 12H), 1.30 (d, J = 6.9 Hz, 12H). ^{13}C{^{1}H} NMR (75 MHz, C_6D_6): δ 163.45, 163.28, 149.24, 141.08, 134.38, 123.78, 123.67, 118.74, 114.96, 93.76, 55.11, 28.61, 24.94, 23.89, 23.80. UV−vis (THF) [λ_{max}, nm (ϵ, M^{-1} cm^{-1})]: 249 (27800), 273 (26800), 352 (24800), 413 (sh, 2700). Anal. Calcd for $C_{66}H_{86}N_6Cu_2$: C, 72.34; H, 7.88; N, 6.84. Found: C, 72.17; H, 8.50; N, 6.82.

Isolation of Solid L^1CuO_2. A solid sample for XAS measurements was obtained as follows. Solid L^1Cu(MeCN) (0.198 g, 0.379 mmol) was dissolved in acetone (∼20 mL). The solution was cooled to 193 K, and dry O_2 was bubbled through it for approximately 30 min. The solution became bright green, and a green precipitate began to form. The mixture was then stored at 193 K overnight. The acetone mother liquor was removed via cannula to leave behind a green solid. This solid was washed with pentane at 193 K several times and then dried under vacuum while maintaining the temperature at 193 K (∼0.135 g, 69%).

X-ray Crystallography. (A) [(L^1Cu)$_2$(*p*-NC-C_6H_4-CN)]. Data collection details are provided in Table S2 and in the Supporting Information as a CIF. The structure was solved using Sir97[33] and refined using SHELXL-97.[34] A highly disordered solvent molecule (on a $\bar{4}$ position) could not be modeled appropriately and was removed using the PLATON program, SQUEEZE function.[35] A total of 53 electrons in a volume of 531.2 Å^3 in the unit cell were determined. These electrons were distributed among two main voids with volumes of 167 and 168 Å^3 containing 26 electrons each, corresponding to two solvent molecules per cell. However, the identity of the solvent based on the volume of the void space and number of electrons could not be determined. As a result, various fields in Table S2 are incorrect (e.g., formula, formula weight, and density). One isopropyl group (C24, C25, C26) contains a slight disorder, but attempts to model this disorder were unsuccessful.

(B) [L^1Cu(*p*-NC-C_6H_4-OMe). Data collection details are provided in the Supporting Information (Table S2 and a CIF). The structure was solved using Sir97[33] and refined using SHELXL-97.[34] The asymmetric unit contains two independent molecules, and in one molecule (A), the methoxy group is disordered over two positions (72:28). This disorder was modeled by splitting the OMe unit into two parts; O1A was split into O1A and O1A′ using identical coordinates and displacement parameters (applying EADP and EXYZ commands), and C37A was split into C37A and C37A′.

(C) L^2CuO_2. Crystals suitable for X-ray crystallography were grown at 193 K from a 50:50 THF/pentane solution of L^2Cu(MeCN), which was treated with O_2 at 193 K. A crystal (approximate dimensions of 2.0 × 0.02 × 0.01 mm) was placed onto the tip of a 0.1 mm diameter glass capillary and mounted on a Bruker Kappa SMART 6000 system for data collection at 100(1) K. The data collection was carried out using 0.5500 Å radiation (double-diamond monochromator) with a frame time of 1 s and a detector distance of 4.9 cm at APS ChemMatCARS 15-ID-C. A randomly oriented region of reciprocal space was surveyed to the extent of 2.0 hemispheres and to a resolution of 0.76 Å. The beam was 100 × 100 μ^2 and was centered on a section of the 2 mm long needle. One set of frames was collected with 0.30° steps in a complete rotation of phi. The intensity data were corrected for absorption and decay (SADABS).[36] Final cell constants were calculated from 3281 strong reflections from the actual data collection after integration (SAINT 6.35A, 2002).[37] Additional crystallographic information is presented in Table S2.

The structure was solved using SHELXS-86 and refined using SHELXL-97.[34] The space group *Imm*2 was determined based on systematic absences and intensity statistics. A direct-methods solution was calculated, which provided most non-hydrogen atoms from the E-map. Full-matrix least-squares difference Fourier cycles were performed, which located the remaining non-hydrogen atoms. All non-hydrogen atoms were refined with anisotropic displacement parameters unless stated otherwise. All hydrogen atoms were placed in ideal

(32) Cramer, C. J.; Tolman, W. B.; Theopold, K. H.; Rheingold, A. L. *Proc. Natl. Acad. Sci. U.S.A.* **2003**, *100*, 3635.
(33) Altomare, A.; Burla, M. C.; Camalli, M.; Cascarano, G.; Giacovazzo, C.; Guagliardi, A.; Moliterni, G. G.; Polidori, R.; Spagna, R. *J. Appl. Crystallogr.* **1998**, *119*, 115.
(34) *SHELXTL-Plus*, version 6.10; Bruker Analytical X-ray Systems: Madison, WI.
(35) Spek, A. L. *Acta Crystallogr.* **1990**, *A46*, C34. (b) Spek, A. L. *PLATON*, A Multipurpose Crystallographic Tool; Utrecht University: Utrecht, The Netherlands, 2000.
(36) For an empirical correction for absorption anisotropy, see: Blessing, R. *Acta Crystallogr.* **1995**, *A51*, 33−38.
(37) *SAINT*, version 6.35A; Bruker Analytical X-ray Systems: Madison, WI.

positions and refined as riding atoms with relative isotropic displacement parameters.

X-ray Absorption Spectroscopy. X-ray absorption spectra of L^1CuO_2 were measured at the Stanford Synchrotron Radiation Laboratory on the focused 16-pole 2.0 T wiggler beam line 9-3 and the unfocused 8-pole 1.8 T wiggler beam line 7-3 under standard ring conditions of 3 GeV and 60−100 mA. A Si(220) double-crystal monochromator was used for energy selection. A Rh-coated harmonic rejection mirror and a cylindrical Rh-coated bent focusing mirror were used for beam line 9-3, whereas the monochromator was detuned 50% at 9987 eV on beam line 7-3 to reject components of higher harmonics. The solid sample was finely ground with BN into a homogeneous mixture and pressed into a 1 mm aluminum spacer between X-ray transparent Kapton tape at dry ice temperature and under a N_2 atmosphere. The sample was immediately frozen thereafter and stored under liquid N_2. During data collection, it was maintained at a constant temperature of 10 K using an Oxford Instruments CF 1208 liquid helium cryostat. Transmission mode was used to measure data to $k = 16$ Å^{-1}, which was possible in the absence of any Zn contamination. Internal energy calibration was accomplished by simultaneous measurement of the absorption of a Cu foil placed between two ionization chambers situated after the sample. The first inflection point of the foil spectrum was assigned to 8980.3 eV. Data represented here is a three-scan average spectrum, which was processed by fitting a second-order polynomial to the pre-edge region and subtracting this from the entire spectrum as background. A three-region spline of orders 2, 3, and 3 was used to model the smoothly decaying post-edge region. The data were normalized by subtracting the cubic spline and by assigning the edge jump to 1.0 at 9000 eV using the SPLINE program in the XFIT suite of programs (Dr. Paul Ellis, SSRL). Theoretical EXAFS signals, $\chi(k)$, were calculated using FEFF (version 7.0)[38,39] and fit to the data using EXAFSPAK (G. N. George, SSRL). The structural parameters that varied during the fitting process were the bond distance (R) and the bond variance (σ^2), which is related to the Debye−Waller factor resulting from thermal motion and static disorder. The nonstructural parameter, E_0 (the energy at which $k = 0$), was also allowed to vary but was restricted to a common value for every component in a given fit. Coordination numbers were systematically varied in the course of the fit but were fixed within a given fit.

Stopped-Flow Kinetics. All manipulations of the copper(I) complexes and their solutions were done inside a Vacuum Atmospheres glovebox with argon or using Hamilton airtight syringes. Tetrahydrofuran (THF) was purified by purging with ultrapure argon and passing through a column of activated anhydrous alumina under an argon atmosphere. Nitriles were purchased from Aldrich or Acros in the highest purity grade available and degassed before taking into the glovebox. Saturated solutions of O_2 in THF (10 mM) were prepared by bubbling dry O_2 gas through argon-saturated THF in a syringe at 293 K for 15 min.[40] Solutions of O_2 with smaller concentrations were prepared by diluting the 10 mM O_2 solution with argon-saturated THF using graduated gastight syringes. Kinetic measurements were performed using a Hi-Tech Scientific (Salisbury, Wiltshire, U.K.) SF-43 multimixing anaerobic cryogenic stopped-flow instrument combined with a Hi-Tech Scientific Kinetascan diode array rapid scanning unit. The solutions of L^1Cu(RCN) in THF or THF/RCN and O_2 in THF were separately cooled to a low temperature (193−233 K) and mixed in a 1:1 volume ratio. The mixing cell (1 cm) was maintained at ±0.1 K, and the mixing time was ∼10 ms. Concentrations of all reagents are reported at the onset of the reaction (after mixing) and corrected for the 1:1 dilution. No correction for the temperature contraction of solvent was applied in this work. Dioxygen (1.25−5.0 mM) was always taken in large excess to the copper(I) complexes (0.1−0.4 mM). In all kinetic experiments, a series of 5−7 shots gave standard deviations within 5%, with overall reproducibility within 10%. Data analysis was performed with the IS-2 Rapid Kinetics Software (Hi-Tech Scientific) for kinetic traces at a single wavelength or with the Specfit program (BioLogic Science Instruments, Grenoble, France) for global fitting of the spectral changes acquired in a diode array mode. Standard deviations of the rate constants and activation parameters were either calculated by the Specfit program or determined from linear fits using the method of least squares.[41]

Computational Methods. An earlier study[42] modeled η^2 1:1 Cu−O_2 adducts supported by a simplified version of the full β-diketiminate ligands L^1 and L^2. Geometries obtained from restricted and unrestricted density functional theory (DFT) methods were found to be optimal for the singlet and triplet states of the Cu−O_2 adducts, respectively, while the multideterminantal character of the singlet adducts mandated the use of multireference second-order perturbation theory for the prediction of system energies. The computational protocol employed herein is based closely upon these findings.

DFT Methods. Geometry optimizations were performed with DFT using the B3LYP functional[43−45] as implemented in the Jaguar, version 5.0, suite of ab initio quantum chemistry programs.[46] A restricted (RDFT) methodology was used for all species where dioxygen is not present and for the singlet Cu−O_2 adducts. Unrestricted (UDFT) wave functions were obtained for molecular O_2 and the triplet Cu−O_2 adducts. The 6-31G** basis set was used for all atoms, with the exception of the Los Alamos lacvp** basis set[47−49] (including an effective core potential and polarization functions) for the one Cu atom. Mappings along reaction coordinates were performed by freezing at least one interatomic distance and by optimizing all other degrees of freedom. Maxima along these coordinates were used as starting structures for quadratic synchronous transit (QST) transition-state searches.[50]

Vibrational frequencies were determined analytically using a truncated version of L^1 obtained by removing the four isopropyl groups, replacing them with hydrogen atoms, and optimizing the positions of those hydrogen atoms while fixing the rest of the structure. Calculation of vibrational frequencies not only allowed for verification of the computed intermediates and transition states as bona fide stationary points but also enabled zero-point energy, enthalpy, and entropy corrections to be made and, therefore, free energies for all species to be obtained. To calculate O−O stretching frequencies, a triple-ζ quality basis set (6-311G** for all atoms, except lacv3p** for Cu[47−49]) and a scaling factor of 0.97[51] were employed, as these steps have been shown to lead to increased reliability in the computational result.[32]

Single-point solvation energies were calculated with a self-consistent reaction field method using the Poisson−Boltzmann solver implemented in Jaguar.[52,53] The dielectric constant, ϵ, for tetrahydrofuran (THF), used as the solvent in order to compare with available experimental kinetics data, was computed from a quadratic fitting of ϵ to the absolute temperature T (eq 1), where a, b, and c are 30.739, −0.12946, and 0.000 171 95, respectively.[54] The dielectric constant for THF is then 7.43 at 298 K and 10.42 at 223 K (the experimental reaction

(38) Mustre de Leon, J.; Rehr, J. J.; Zabinsky, S. I.; Albers, R. C. *Phys. Rev. B* **1991**, *44*, 4146.
(39) Rehr, J. J.; Mustre de Leon, J.; Zabinsky, S. I.; Albers, R. C. *J. Am. Chem. Soc.* **1991**, *113*, 5135.
(40) Battino, R. *Oxygen and Ozone*; Battino, R., Ed.; Pergamon Press: New York, 1981; Vol. 7.
(41) Skoog, D. A.; Leary, J. J. *Principles of Instrumental Analysis*, 4th ed.; Saunders: Fort Worth, TX, 1992.
(42) Gherman, B. F.; Cramer, C. J. *Inorg. Chem.* **2004**, *43*, 7281.
(43) Johnson, B. G.; Gill, P. M. W.; Pople, J. A. *J. Chem. Phys.* **1993**, *98*, 5612.
(44) Becke, A. D. *J. Chem. Phys.* **1993**, *98*, 1372.
(45) Lee, C. T.; Yang, W. T.; Parr, R. G. *Phys. Rev. B* **1988**, *37*, 785.
(46) *Jaguar 5.0*; Schrodinger, LLC: Portland, OR, 2002.
(47) Hay, P. J.; Wadt, W. R. *J. Chem. Phys.* **1985**, *82*, 270.
(48) Wadt, W. R.; Hay, P. J. *J. Chem. Phys.* **1985**, *82*, 284.
(49) Hay, P. J.; Wadt, W. R. *J. Chem. Phys.* **1985**, *82*, 299.
(50) Peng, C. Y.; Schlegel, H. B. *Isr. J. Chem.* **1993**, *33*, 449.
(51) Bauschlicher, C. W.; Partridge, H. *J. Chem. Phys.* **1995**, *103*, 1788.
(52) Marten, B.; Kim, K.; Cortis, C.; Friesner, R. A.; Murphy, R. B.; Ringnalda, M. N.; Sitkoff, D.; Honig, B. *J. Phys. Chem.* **1996**, *100*, 11775.
(53) Tannor, D. J.; Marten, B.; Murphy, R. B.; Friesner, R. A.; Sitkoff, D.; Nicholls, A.; Ringnalda, M. N.; Goddard, W. A., III.; Honig, B. *J. Am. Chem. Soc.* **1994**, *116*, 11875.

temperature).[55] When computing free energy changes in solution, a correction for translational entropy due to a change in concentration from gas phase (i.e., the concentration at 1 atm, which may be computed from the ideal gas law) to the 1 M standard-state solution concentration was included.[56] In the case that the THF solvent plays an explicit role in a chemical reaction, the concentration of the solvent (determined from its density[57,58] and molecular weight) was factored into the entropy correction.

$$\epsilon(T) = a + bT + cT^2 \quad (1)$$

Multireference Methods. In general, a closed-shell singlet state and a high-spin triplet state can each be described within a single-determinantal formalism. An open-shell singlet, however, cannot be formally expressed in a single-determinantal framework (such as Kohn−Sham DFT) and requires at least two determinants. With regard to $Cu-O_2$ adducts and in particular those possessing Cu(II)−superoxide character, the open-shell singlet state becomes significant since Cu(II)−superoxide is formally a biradical with one electron localized to Cu and another to the O_2 moiety. The multideterminantal character of the singlet $Cu-O_2$ adducts must then be accounted for when these species' energies are calculated. Thus, to obtain accurate energy differences between singlet and triplet states, single-point calculations were performed using multireference second-order perturbation theory (CASPT2).[59] The initial complete active space (CAS) for the reference wave functions consisted of 18 electrons in 12 orbitals, specifically, the valence orbitals/electrons of Cu and the O_2 σ_{2p}, σ_{2p}*, π_{2p}, and π_{2p}* orbitals/electrons. A final (12,9) subspace was obtained by removing orbitals with occupation numbers greater than 1.999 for each geometry under consideration. All CAS and CASPT2 calculations were done with MOLCAS,[60] using a polarized valence double-ζ atomic natural orbital basis set and 17-electron relativistic effective core potential for Cu.

Corrections to the DFT Singlet Energies. CASPT2 calculations were carried out using a simplified version (sans the 2,6-diisopropylphenyl flanking groups and methyl groups on the L^1 backbone) of the full β-diketiminate ligand system in order to make calculations at this level of theory tractable. CASPT2 energies were determined for the singlet ($^1A_1$) and triplet ($^3B_1$) states for the C_{2v} side-on (η^2) adducts over a range of distances between Cu and the O−O midpoint. Differences between the singlet/triplet splittings at the CASPT2 level of theory and from the DFT calculations were then calculated according to eq 2. Assuming the triplet state to be well-described by a single determinant, as in DFT,[61] the relative energy difference between the triplet at the two levels of theory is zero. The Δ quantity in eq 2 is then equal to the relative energy difference between the singlet at the DFT and CASPT2 levels and serves as a correction to the singlet energies produced by DFT, while the triplet correction to the DFT energies is zero. This "CASPT2 correction" to the singlet energy correlates linearly with the Cu−O bond length over a range from 1.85 to 2.41 Å (Figure S1a in the Supporting Information), allowing CASPT2 corrections to be readily determined for any singlet side-on adduct between these two endpoints. A similar linear correlation between the CASPT2 correction and Cu−O bond length from 1.83 to 2.33 Å can be obtained for singlet end-on $Cu-O_2$ adducts (Figure S1b in the Supporting Information). In all cases, the corrections have negative values, indicating that DFT systematically predicts the energies for the significantly multideterminantal singlet states to be too high.

$$\Delta = (^1A_1 - {}^3B_1)_{CASPT2} - (^1A_1 - {}^3B_1)_{DFT} = [(^1A_1)_{CASPT2} - (^1A_1)_{DFT}] - [(^3B_1)_{CASPT2} - (^3B_1)_{DFT}] \quad (2)$$

At infinite Cu−O distances, any CASPT2 correction refers only to molecular dioxygen. Calculations show the correction for singlet dioxygen to be −62.7 kJ mol^{-1}. Corrections at long, yet finite, Cu−O distances were obtained by extrapolating between the dioxygen correction and the maximum CASPT2 correction from the linear correlations. Specifically, such longer range corrections are given by eq 3, where "max correction" is the CASPT2 correction at the last point in the correlation; $O-O_{max}$ and O−O are the oxygen−oxygen bond lengths at that last point in the correlation and in the particular long-range Cu−O structure, respectively, and 1.215 Å is the equilibrium O_2 bond length.

$$(\text{max correction} + 62.7)\left(\frac{O-O - 1.215}{O-O_{max} - 1.215}\right) - 62.7 \quad (3)$$

The CASPT2 corrections are largest at intermediate Cu−O distances, where Cu(II)−superoxo and, hence, biradical and multideterminantal character is the greatest. At short Cu−O distances, the structures increasingly resemble Cu(III)−peroxo, and at long Cu−O distances, the interaction between the Cu(I) complex and dioxygen is relatively minimal. Both latter cases lead to a decrease in the magnitude of the CASPT2 correction to the singlet energy.

A complete listing of individual energies and the precise protocol for computing composite energies, enthalpies, entropies, and free energies in the gas phase and in THF solution are provided in the Supporting Information.

Results

Synthesis. The synthesis, spectroscopic data, and X-ray crystal structures of the complexes LCu(MeCN) (L = L^1 or L^2) were reported previously.[30,31] As described below, substitution of the MeCN ligand by various *para*-substituted benzonitriles was implicated by UV−vis spectroscopic monitoring of stopped-flow kinetic experiments. To confirm that benzonitrile adduct formation occurred, complexes of two members of the series were independently synthesized and characterized. Thus, treatment of $L^1Cu(MeCN)$ in THF with *p*-NC-C_6H_4-CN (0.5 equiv) or *p*-NC-C_6H_4-OMe (1 equiv) yielded [($L^1Cu)_2$-(*p*-NC-C_6H_4-CN)] or L^1Cu(*p*-NC-C_6H_4-OMe), respectively, as solids amenable to analysis by NMR and UV−vis spectroscopy, elemental analysis, and X-ray crystallography (Figure S2 in the Supporting Information).

Solid samples of the O_2 adduct, L^1CuO_2, were prepared by bubbling O_2 through solutions of $L^1Cu(MeCN)$ in acetone at 193 K. The complex L^1CuO_2 precipitated as a green, temperature-sensitive powder. The adduct, L^2CuO_2, was prepared similarly, except it was isolated as crystals suitable for analysis by X-ray diffraction from solutions of THF/pentane (1:1).

X-ray Crystallography. (A) [($L^1Cu)_2$(*p*-NC-C_6H_4-CN)] and L^1Cu(*p*-NC-C_6H_4-OMe). Representations of the X-ray crystal structures of these molecules are shown in Figure S2 (Supporting Information), with selected crystallographic data listed in Table S2 (Supporting Information). Overall, the structures resemble those reported previously for (β-diketiminate)Cu(MeCN) com-

(54) Lide, D. R. *Handbook of Chemistry and Physics*, 84th ed.; CRC Press: Boca Raton, FL, 2003.
(55) These dielectric constant values will not be appreciably altered by the addition of the small amounts of MeCN to the THF solvent used during the synthesis of L^1CuO_2.
(56) Cramer, C. J. *Essentials of Computational Chemistry*, 2nd ed.; John Wiley & Sons: Chichester, 2004.
(57) Carvajal, C.; Tolle, K. J.; Smid, J.; Szwarc, M. *J. Am. Chem. Soc.* **1965**, *87*, 5548.
(58) Metz, D. J.; Glines, A. *J. Phys. Chem.* **1967**, *71*, 1158.
(59) Andersson, K.; Malmqvist, P. A.; Roos, B. O. *J. Chem. Phys.* **1992**, *96*, 1218.
(60) Karlstrom, G.; Lindh, R.; Malmqvist, P. A.; Roos, B. O.; Ryde, U.; Veryazov, V.; Widmark, P. O.; Cossi, M.; Schimmelpfennig, B.; Neogrady, P.; Seijo, L. *Comput. Mater. Sci.* **2003**, *28*, 222.
(61) This assumption is supported by the CASPT2 calculations on the triplets, which show that their multideterminantal wave functions are dominated by a single configuration with a weight of approximately 0.95, with any other contributors having weights <0.015.

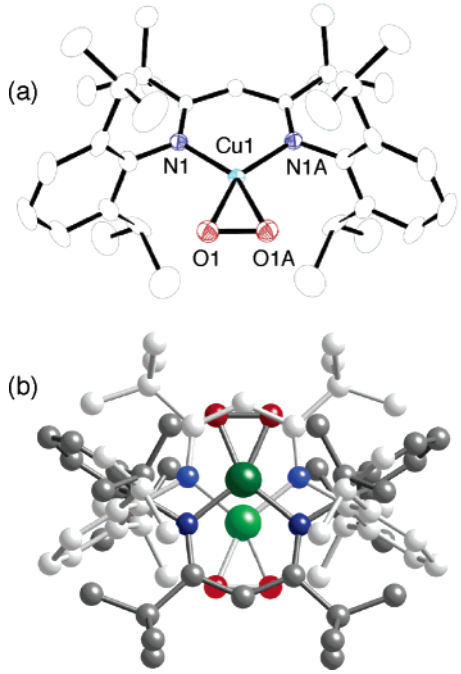

Figure 1. (a) Representation of the X-ray crystal structure of L^2CuO_2, with all non-hydrogen atoms shown as 50% thermal ellipsoids. Selected bond distances (angstroms) and angles (degrees): Cu1−N1, 1.856(6); Cu1−O1, 1.821(5); O1−O1′, 1.392(12); O1−Cu1−O1′, 44.9(4). (b) Illustration of the disorder present in the crystals of L^2CuO_2.

plexes.[29,30] The Cu(I) ions exhibit similar three-coordinate geometries distorted by virtue of the benzonitrile ligand being displaced toward one side of the β-diketiminate ligand L^1. This displacement is characterized by N(L^1)−Cu−N(nitrile) angles for each Cu site that differ by 34−40°. Asymmetry in the coordination of L^1 is evidenced by Cu−N(L^1) distances that differ by 0.07−0.09 Å.

(B) L^2CuO_2. We previously noted that the X-ray crystal structure of L^2CuO_2 contains a whole-molecule disorder, and that the large number of restraints needed to model this disorder affects the precision of the bond lengths and angles.[31] As such, though the crystal structure confirms the η^2-coordination of O_2 to copper, the O−O bond distance of 1.440(16) Å, while consistent with a formulation with significant Cu(III)−peroxo character,[32] can only be deemed approximate. Given the importance of the O−O bond distance in evaluating the electronic structure of the 1:1 adduct, the crystal structure was redetermined using a more powerful synchrotron beam (Figure 1). Selected crystallographic data for the new structure of L^2CuO_2 is given in Table S2 (Supporting Information). With the synchrotron radiation, a higher quality (i.e., more intense) data set was collected; however, the whole-molecule disorder is still evident and the original structure solution still applicable. The Cu−N/O ligand distances are reasonable (i.e., shorter than analogous distances in Cu(I) complexes) and agree well with those determined independently for L^1CuO_2 by EXAFS (see below). Importantly, the improved data set gives a shorter O−O bond distance of 1.392(12) Å, which more closely resembles the value determined previously using DFT calculations (1.376 Å).[31]

Nonetheless, this distance should still be considered an approximation due to the number of restraints needed to model the disorder, which warrants explanation. The original structure was solved in space group *Imm*2, although several others, including *I*222 and $I2_12_12_1$, were evaluated. Only one-fourth of the molecule is unique, with the rest generated by symmetry operations. Upon collection of the new data set, other space groups were considered but were again all rejected in favor of *Imm*2. The entire molecule is disordered over two positions in a 66:34 ratio (Figure 1b). Several possible twinning modes were evaluated, and none led to a model removing the disorder. While some THF solvent molecules could be located by the difference Fourier map, all solvent atoms were removed using the PLATON/SQUEEZE program,[35] which resulted in a better model. The void space suggests approximately six THF molecules, or three per copper complex. The structure contains solvent channels that minimize direct van der Waals contacts between copper complexes in adjacent columns. This loose packing allows complexes to fill the space in both directions, and it is the averaging of the complexes in opposing directions that leads to the static whole-molecule disorder.

X-ray Absorption Spectroscopy. (A) Cu K-Edges. Experimental insight into the oxidation state of the copper ion in the 1:1 Cu−O_2 adducts was obtained through Cu K-edge XAS. Previous studies of the copper K-edge XAS data for series of Cu(II) and Cu(III) complexes showed that this method can clearly distinguish these oxidation levels.[62] Notably, a prominent pre-edge 1s → 3d transition is centered at ∼8981 eV for Cu(III), approximately 2 eV higher than the energy of this transition in Cu(II) complexes. This distinction has been found to hold irrespective of the ligands, and thus is analytically useful for distinguishing these oxidation levels, even when counterparts with the same ligand set but a different oxidation state are unavailable for comparison.

The normalized X-ray absorption K-edge spectrum of solid L^1CuO_2 is shown in Figure 2a. The pre-edge feature observed at ∼8981 eV is a low-intensity (dipole-forbidden) quadrupole-allowed transition, which gains intensity due to 4p orbital mixing into the d-manifold as the molecule deviates toward lower symmetry relative to a centrosymmetric species. The maximum of the pre-edge appears at ∼8980.7 eV (inset). A characteristic 1s → 4p + LMCT shakedown transition[62b,63] is observed on the rising edge at ∼8986.7 eV. In Figure 2b, the Cu-edge spectrum of L^1CuO_2 is compared to previously reported[62a] spectra for the dicopper(II,II) complex, $[L^3{}_2Cu_2(\mu\text{-}OH)_2]^{2+}$, and the dicopper(III,III) compound, $[L^3{}_2Cu_2(\mu\text{-}O)_2]^{2+}$ (L^3 = *N,N,N′,N′*-tetraethylethylenediamine). The latter compounds exhibit data typical for their assigned oxidation states, with 1s → 3d transitions at ∼8979 ± 0.3 eV for Cu(II) and at ∼8981 ± 0.5 eV for Cu(III). It is evident (inset) that the pre-edge feature for L^1CuO_2 at ∼8980.7 eV falls in the Cu(III) region, approximately 1.5−2 eV higher than that for Cu(II) complexes, and is quite similar to that of $[L^3{}_2Cu_2(\mu\text{-}O)_2]^{2+}$.

(B) EXAFS. In lieu of X-ray crystallographic data (only available for L^2CuO_2), structural information for L^1CuO_2 was obtained by EXAFS analysis. The k^3-weighted EXAFS data and their Fourier transform are shown in Figure 3. Theoretical phase and amplitude parameters for the fit were generated by

(62) DuBois, J. L.; Mukherjee, P.; Collier, A. M.; Mayer, J. M.; Solomon, E. I.; Hedman, B.; Stack, T. D. P.; Hodgson, K. O. *J. Am. Chem. Soc.* **1997**, *119*, 8578. (b) DuBois, J. L.; Mukherjee, P.; Stack, T. D. P.; Hedman, B.; Solomon, E. I.; Hodgson, K. O. *J. Am. Chem. Soc.* **2000**, *122*, 5775.
(63) Kau, L.-S.; Spira-Solomon, D. J.; Penner-Hahn, J. E.; Hodgson, K. O.; Solomon, E. I. *J. Am. Chem. Soc.* **1987**, *109*, 6433.

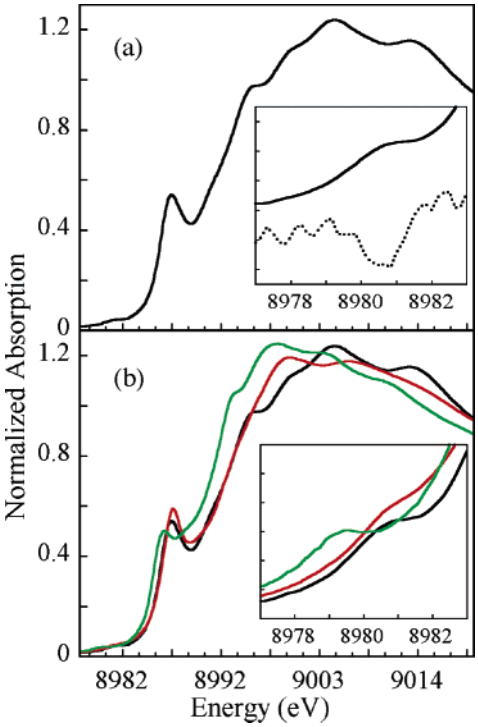

Figure 2. (a) Normalized Cu K-edge X-ray absorption spectrum of L^1CuO_2. The inset shows the pre-edge region (—) and its second derivative (- - -). (b) Overlay of the normalized Cu K-edge X-ray absorption spectra of L^1CuO_2 (black), the previously published[62] data of the dicopper(II,II) complex $[L^3{}_2Cu_2(\mu\text{-}OH)_2]^{2+}$ (green), and the dicopper(III,III) complex $[L^3{}_2Cu_2(\mu\text{-}O)_2]^{2+}$ (red), where L^3 = *N*,*N*,*N*′,*N*′-tetraethylethylenediamine. The pre-edge region is expanded in the inset.

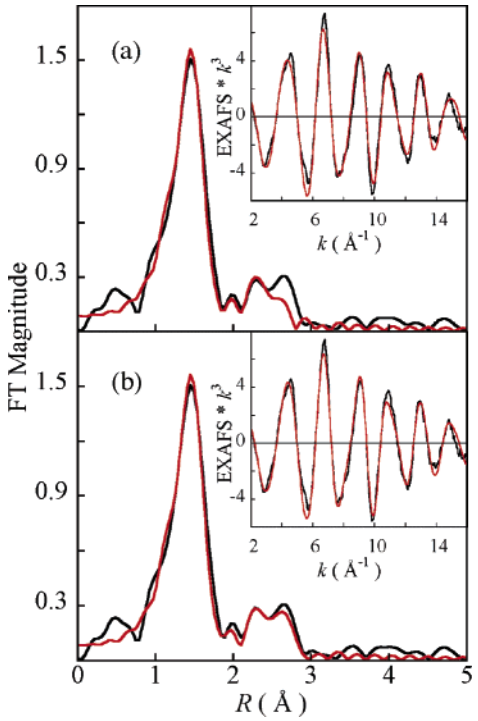

Figure 3. EXAFS data (black), fits (red), and the corresponding Fourier transforms for L^1CuO_2, including (a) only single scattering (SS) and (b) both SS and multiple scattering (MS) pathways.

FEFF,[38,39] using the crystallographic parameters for L^2CuO_2. Good fits to the EXAFS were obtained by including a first shell of four O/N scatterers and a second shell including single scattering (SS), and/or multiple scattering (MS) pathways from the rigid β-diketiminate ligand system. Figure 3a shows EXAFS fits and the corresponding Fourier transforms, including only SS pathways, while Figure 3b shows the complete fit involving both SS and MS paths. The best fit is obtained with four Cu−N/O distances at 1.83 Å, four Cu−C at 2.79 Å, one Cu−C at 3.17 Å, and a MS pathway Cu−N−C at 2.98 Å (Table 1). The σ^2 value for the MS pathway is linked to that of the corresponding Cu−C SS pathway, and its inclusion improved the fit significantly, as shown in the comparison of the Fourier transforms (Figure 3b). Each atom in the β-diketiminate−Cu ring contributes to the EXAFS signal, whereas the aryl substituents (except for the carbon directly attached to the N atom) do not contribute significantly, most likely due to the relative rigidity of the six-membered β-diketiminate−Cu ring. In summary, the good fits and resulting interatomic distances obtained from the EXAFS data for L^1CuO_2 corroborate the distances obtained by X-ray crystallography for L^2CuO_2. Thus, the EXAFS results support the crystallographic conclusions, notwithstanding the disorder problems that adversely influence the precision of the X-ray diffraction results.

Table 1. EXAFS Curve-Fitting Results

fit no.		R (Å)[a]	σ^2 (Å^2)[b]	E_0 (eV)	F[c]
1	4 Cu−N/O	1.83	33	−7.7	0.31
2	4 Cu−N/O	1.83	37	−7.05	0.20
	4 Cu−C	2.80	34		
3	4 Cu−N/O	1.83	34	−6.90	0.18
	4 Cu−C	2.80	42		
	8 Cu−N−C	2.98	42[d]		
	1 Cu−C	3.17	14		

[a] Estimated standard deviation for the distances are on the order of ±0.02 Å. [b] The σ^2 values are multiplied by 1×10^5. [c] Error is given by $\sum[(\chi_{obs} - \chi_{calcd})^2k^6]/\sum[(\chi_{obs})^2k^6]$. [d] The σ^2 factor of the MS path is linked to that of the corresponding SS path.

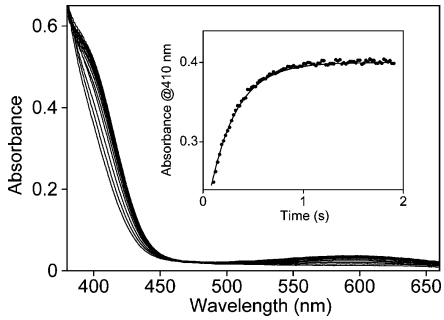

Figure 4. Stopped-flow time-resolved UV−vis spectra of the reaction of $L^1Cu(MeCN)$ (0.25 mM) with O_2 (~5 mM) in THF at 203 K recorded every 0.02 s (approximately every 4th spectrum shown). Inset: kinetic trace at 410 nm with single-exponential fit to $A_t = A_\infty - (A_\infty - A_0)\exp(-kt)$, $k = 3.73\ s^{-1}$. A similar plot at 600 nm is shown in Figure S3 (Supporting Information).

Oxygenation Kinetics. The kinetics of the reaction of $L^1Cu(MeCN)$ with O_2 in THF or THF/MeCN mixtures (0.3−5% MeCN by volume) at low temperatures (193−233 K) were studied using the stopped-flow technique with time-resolved UV−vis spectroscopic monitoring. As shown in Figure 4, the spectrum of yellow $L^1Cu(MeCN)$ converts upon oxygenation to that of green L^1CuO_2 with no accumulation of intermediates. The yield of L^1CuO_2, as indicated by final absorbance values (approaching 100%), was the same with or without added MeCN, consistent with an irreversible oxygenation reaction and

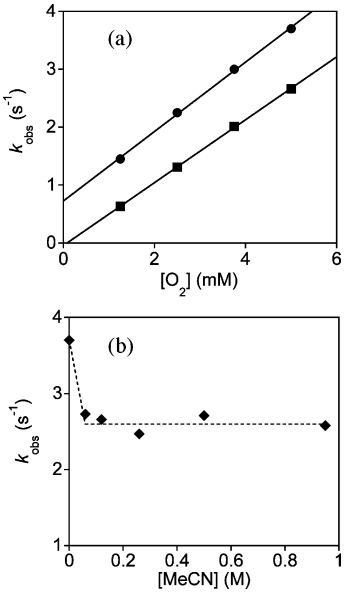

Figure 5. Plots of the observed pseudo-first-order rate constant for the oxygenation of $L^1Cu(MeCN)$ (0.25 mM) at $T = 203$ K, (a) at variable [O_2] in neat THF (●) and THF/MeCN (■) ([MeCN] = 60 mM) and (b) at variable [MeCN] and constant [O_2] = 5 mM.

in agreement with batch experiments wherein the amount of L^1CuO_2 was found to be unperturbed by removal of O_2 from solution. Under excess O_2, the spectral changes with time are fit well to a single exponential (Figure 4 inset and Figure S3 in the Supporting Information) to yield a pseudo-first-order rate constant (k_{obs}) that is independent of the initial concentration of $L^1Cu(MeCN)$ (Table S3 in the Supporting Information). These data indicate a first-order dependence on [$L^1Cu(MeCN)$], eq 4.

$$\frac{\partial[L^1CuO_2]}{\partial t} = -\frac{\partial[L^1Cu(MeCN)]}{\partial t} = k_{obs}[L^1Cu(MeCN)] \quad (4)$$

The dependence on [O_2] is more complicated and is affected by the presence of MeCN, which moderately decreases k_{obs} (Figure 5 and Figure S4 and Table S4 in the Supporting Information). For instance, under the conditions $T = 203$ K, $[L^1Cu(MeCN)]_0 = 0.25$ mM, and maximum available excess [O_2] (5 mM), the k_{obs} value in neat THF of 3.7 ± 0.1 s^{-1} changes to 2.66 ± 0.06 s^{-1} in the presence of 120 mM MeCN. The latter value of k_{obs} is unchanged by further increases in $[MeCN]_0$ (up to 950 mM, 5 vol %), indicating saturation behavior and a zero-order dependence in [MeCN] when in excess. In THF/MeCN mixtures, plots of k_{obs} versus [O_2] are linear with zero intercepts at all temperatures (193−233 K, Figure 6a). Thus, in the presence of MeCN, the oxygenation displays a first-order dependence on [O_2] with an overall second-order rate law (eqs 5 and 6).

$$k_{obs}^{THF/MeCN} = k_A[O_2] \quad (5)$$

$$\frac{\partial[L^1CuO_2]}{\partial t} = -\frac{\partial[L^1Cu(MeCN)]}{\partial t} = k_A[L^1Cu(MeCN)][O_2] \quad (6)$$

In neat THF, however, plots of k_{obs} versus [O_2] also are linear, but with significant positive *y*-intercepts (Figures 5 and 6b). In

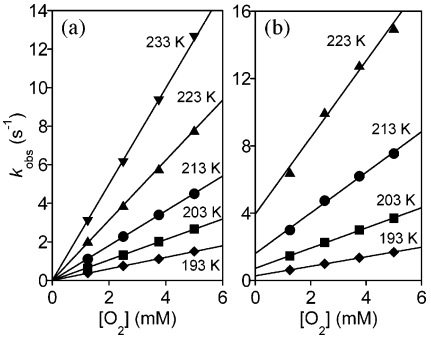

Figure 6. Plots of observed pseudo-first-order rate constants for the oxygenation of $L^1Cu(MeCN)$ (0.25 mM) at various temperatures as a function of [O_2] in (a) THF/MeCN (v/v 160:1; [MeCN] = 0.12 M) and (b) neat THF. The data presented in these plots are listed in Table S4 (Supporting Information).

Scheme 1

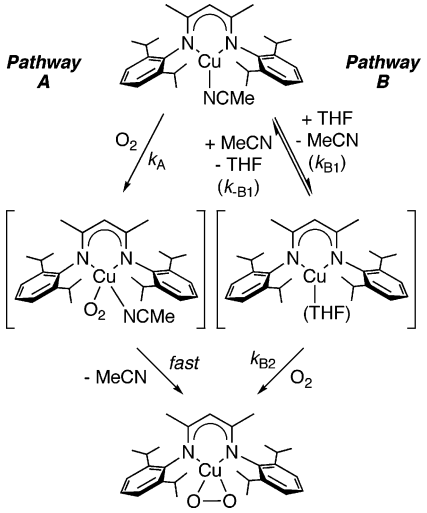

addition, the rate constants in neat THF are systematically higher than those in THF/MeCN (Figure S4 and Table S4 in the Supporting Information). These results indicate that there is an additional oxygenation pathway operative in neat THF that exhibits a zero-order dependence on [O_2], such that the overall rate law has two terms (eqs 7 and 8).

$$k_{obs}^{THF} = k_A[O_2] + k_B \quad (7)$$

$$\frac{\partial[L^1CuO_2]}{\partial t} = -\frac{\partial[L^1Cu(MeCN)]}{\partial t} = k_A[L^1Cu(MeCN)][O_2] + k_B[L^1Cu(MeCN)] \quad (8)$$

By analogy to the results of classic studies of ligand substitution reactions of square planar complexes that yielded rate laws of identical form to eq 8 (see Discussion),[64] we propose a dual-pathway mechanism (Scheme 1). The first and rate-limiting step of pathway A is a direct bimolecular reaction of $L^1Cu(MeCN)$ with O_2, where adduct $L^1Cu(MeCN)(O_2)$ may be considered as a transition state or an unstable intermediate that releases MeCN and converts to L^1CuO_2 in a post-rate-limiting step(s). In pathway B, the first and rate-limiting step is solvolysis of $L^1Cu(MeCN)$ to yield a highly reactive intermediate

(64) Wilkins, R. G. *Kinetics and Mechanism of Reactions of Transition Metal Complexes*, 2nd ed.; VCH: Weinheim, Germany, 1991; pp 232−243 and references therein.

Table 2. Selected Kinetic Parameters for Oxygenation of Mononuclear Cu(I) Complexes Leading to 1:1 Cu−O_2 Adducts[a]

Cu(I) complex	solvent	k_{on} (223 K)[b]	$\Delta H^{\ddagger}$ (kJ mol^{-1})	$\Delta S^{\ddagger}$ (J K^{-1} mol^{-1})	ref
L^1Cu(MeCN), pathway A[c]	THF−MeCN or THF	1560 ± 19	18 ± 2 14.9 (t)	−100 ± 10 −108 (t)	this work
L^1Cu(MeCN), pathway B[d]	THF	3.95 ± 0.59[e]	30 ± 2 2 7.2 (t)	−98 ± 10 −101.0 (t)	this work
L^iPr3Cu(MeCN)	Me_2CO	5.2[f]	37.2 ± 0.5	−62 ± 2	74
(Me_6tren)Cu(EtCN)	EtCN	(8.7 ± 0.4) × 10^5	17.1 ± 0.6	−52 ± 3	22b
(TMPA)Cu(EtCN)	EtCN	(5.0 ± 0.3) × 10^5	31.6 ± 0.5	10 ± 3	27
(TMPA)Cu(THF)	THF	3.4 × 10^8 [f]	7.6	−45	28

[a] All are experimental values, except those denoted by "t", which are derived from theoretical calculations. Abbreviations: L^iPr3 = 1,4,7-triisopropyl-1,4,7-triazacyclononane, Me_6tren = hexamethyltriaminoethylamine, TMPA = tris(pyridylmethyl)amine. [b] Unless noted otherwise, units are in M^{-1} s^{-1}. [c] Parameters determined from experiments in THF/MeCN (v/v 160:1; [MeCN] = 0.12 M). [d] Parameters refer to the solvolysis reaction (exchange of THF for MeCN), not the oxygenation. Thus, k_{on} refers to $k_B = k_{B1}$ (eqs 8 and 9). [e] Units are in s^{-1}. [f] Calculated from the published activation parameters.

L^1Cu(THF) that is subsequently scavenged rapidly by O_2; thus, pathway B is kinetically independent of [O_2]. Assuming that L^1Cu(THF) is a steady-state intermediate, the mechanism in Scheme 1 is described by the rate law in eq 9, which can be shown to be consistent with the rate laws determined experimentally under the different reaction conditions used. Thus, with excess O_2 and in neat THF (no added MeCN), k_{-B1}[MeCN] ≪ k_{B2}[O_2], and eq 9 reduces to the experimentally determined eq 8, where $k_B = k_{B1}$. When a large excess of MeCN is present, k_{-B1}[MeCN] ≫ $k_{B1}k_{B2}$[L^1Cu(MeCN)][O_2], and the second term of eq 9 approaches zero, such that eq 9 reduces to eq 6. In other words, in the presence of excess MeCN, pathway B is effectively shut down because nearly all L^1Cu(THF) is converted to L^1Cu(MeCN), and the oxygenation process proceeds entirely through pathway A.

$$\frac{\partial[L^1CuO_2]}{\partial t} = -\frac{\partial[L^1Cu(MeCN)]}{\partial t} = k_A[L^1Cu(MeCN)][O_2] + \frac{k_{B1}k_{B2}[L^1Cu(MeCN)][O_2]}{k_{-B1}[MeCN] + k_{B2}[O_2]} \quad (9)$$

Activation parameters for both pathways A (k_A) and B ($k_B = k_{B1}$) were obtained from Eyring plots for the respective rate constants measured over the temperature range T = 193−233 K (Figure S5 and Table S5 in the Supporting Information, and Table 2). Associative mechanisms for the rate-determining steps of both pathways are supported by the low $\Delta H^{\ddagger}$ and large negative $\Delta S^{\ddagger}$ values. Further interpretations of the activation parameters are presented in the Discussion.

To obtain deeper insight into the nature of the transition state for the direct oxygenation pathway A, we sought to examine how the kinetic behavior is influenced by variation of ligand electronic properties. Rather than varying the attributes of L^1, which would require extensive synthetic effort, we focused on replacing the readily exchanged MeCN ligand with a series of *para*-substituted benzonitriles (*p*-X-C_6H_4-CN, X = OMe, Me, H, F, Cl, CN). On the basis of the kinetic results for L^1Cu(MeCN), we reasoned that addition of excess *p*-X-C_6H_4-CN to L^1Cu(MeCN) in THF would convert most of L^1Cu(MeCN) to the adduct L^1Cu(NCC_6H_6X) and suppress a solvolytic oxygenation mechanism (pathway B), thus leaving direct reaction of O_2 (pathway A) as the only route to L^1CuO_2. Importantly, in pathway A, the *p*-X-C_6H_4-CN ligand would be lost only after the rate-limiting step of the oxygenation reaction, so that its electronic effects would be manifested by differences in measurable rate constants.

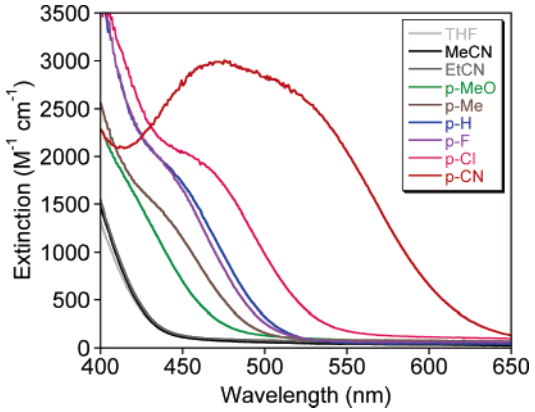

Figure 7. UV−vis spectra at 203 K of L^1Cu(MeCN) (0.2−0.5 mM) in the presence of excess RCN (100 mM) in THF, where R = Me, Et, and *p*-X-C_6H_4 (X = OMe, Me, F, H, Cl, CN).

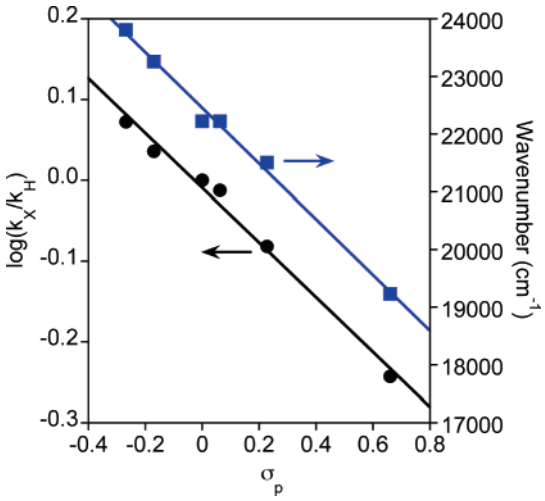

Figure 8. Correlations of the Hammett substituent constants (σ_p) and the energies of the MLCT bands (shoulders, ■) and the pseudo-first-order rate constants for oxygenation of solutions of L^1Cu(MeCN) in the presence of excess *p*-X-C_6H_4-CN (X = OMe, Me, F, H, Cl, CN; 100 mM) (●).

Addition of excess *p*-X-C_6H_4-CN (200 equiv) to solutions of L^1Cu(MeCN) in THF (0.2−0.5 mM) at 203 K resulted in dramatic color and UV−vis spectral changes indicative of the formation of complexes L^1Cu(NCC_6H_6X) (Figure 7). An intense absorbance (ϵ = 1000−3000 M^{-1} cm^{-1}) above 400 nm developed, which shifted hypsochromically with increasing electron-withdrawing capabilities of the substituent X. Indeed, the energy of the absorption feature is linearly correlated with the substituent Hammett constants (σ_p, Figure 8, blue squares), with a negative slope consistent with assignment of the

Table 3. Values of Pseudo-First-Order Rate Constants for Oxygenation of [L^1Cu(RCN)] Complexes[a]

solvent	copper(I) species	k_{obs} (s^{-1})
THF only	[L^1Cu (MeCN)] + [L^1Cu(THF)]	3.7 ± 0.1
MeCN in THF	[L^1Cu(MeCN)]	2.66 ± 0.06
EtCN in THF	[L^1Cu(EtCN)]	2.25 ± 0.05
p-MeO-C_6H_4-CN in THF	[L^1Cu(*p*-MeO-C_6H_4-CN)]	1.24 ± 0.05
p-Me-C_6H_4-CN in THF	[L^1Cu(*p*-MeC_6H_4-CN)]	1.14 ± 0.05
PhCN in THF	[L^1Cu(PhCN)]	1.05 ± 0.05
p-F-C_6H_4-CN in THF	[L^1Cu(*p*-F-C_6H_4-CN)]	1.02 ± 0.03
p-Cl-C_6H_4-CN in THF	[L^1Cu(*p*-Cl-C_6H_4-CN)]	0.87 ± 0.03
p-NC-C_6H_4-CN in THF	[L^1Cu(*p*-NC-C_6H_4-CN)]	0.6 ± 0.2

[a] Solutions were prepared by dissolving solid complex **1** in THF, with $[RCN]_0 = 50$ mM. Conditions: $T = 203$ K, $[\mathbf{1}]_0 = 0.25$ mM, $[O_2]_0 = 5$ mM.

absorption as a metal-to-ligand charge-transfer transition (MLCT, Cu(I) → *p*-X-C_6H_4-CN). No discernible spectral changes occurred when excess EtCN was added to L^1Cu(MeCN) in THF, consistent with indistinguishable UV−vis spectra for L^1Cu(MeCN) and L^1Cu(EtCN), as noted previously for other Cu(I) adducts of aliphatic nitriles.[26a,27]

Final corroboration of the formation of L^1Cu(NCC_6H_6X) in the L^1Cu(MeCN)/*p*-X-C_6H_4-CN mixtures came from the independent isolation and structural characterization of L^1Cu(*p*-CN-C_6H_4-OMe), the UV−vis spectrum of which matched that obtained in the mixing experiments. We note that the spectrum of the isolated dinuclear complex [(L^1Cu)$_2$(*p*-NC-C_6H_4-CN)] was perturbed relative to that seen in the kinetics experiments, wherein *p*-NC-C_6H_4-CN was in large excess relative to L^1Cu(MeCN). However, addition of excess *p*-NC-C_6H_4-CN to the dicopper complex [(L^1Cu)$_2$(*p*-NC-C_6H_4-CN)] resulted in a shift of the intense absorbance feature to approximately the same position as in the kinetics experiments, indicating conversion of the isolated dicopper adduct to the monocopper species L^1Cu(*p*-NC-C_6H_4-CN) in THF in the presence of an excess of the benzonitrile.

Exposure of the solutions comprising L^1Cu(MeCN) and 200 equiv of *p*-X-C_6H_4-CN in THF to O_2 resulted in rapid bleaching of the intense low-energy absorption features to yield a final spectrum identical to that previously identified for L^1CuO_2 (Figure S6 in the Supporting Information). Stopped-flow kinetic studies of the oxygenation reaction in THF at $T = 203$ K with $[L^1Cu(MeCN)]_0 = 0.25$ mM, $[O_2]_0 = 5.0$ mM (excess), and $[p\text{-X-}C_6H_4\text{-CN}]_0 = 50$ mM, yielded single-exponential absorbance versus time curves, for which fits provided pseudo-first-order rate constants, k_{obs} (eqs 5 and 6, Table 3). The k_{obs} values for the adducts of *p*-X-C_6H_4-CN are all smaller than those for L^1Cu(MeCN) itself and for L^1Cu(MeCN) in the presence of EtCN, with the trend $k_{obs}^{MeCN} > k_{obs}^{EtCN} > k_{obs}^{p-X-C6H4-CN}$ being consistent with steric influences on the rate-determining attack of O_2 at the copper center. The trends within the series *p*-X-C_6H_4-CN were most illuminating, however. The rate constants decreased with increasing electron-withdrawing capabilities of the X substituent, yielding a linear Hammett correlation with $\rho = -0.34$ (Figure 8, black circles). These data show that positive charge develops at the copper site in the activated complex during the rate-limiting step of the oxygenation reaction, consistent with the direct associative pathway A (Scheme 1) involving coordination of the nitrile in the activated complex and some degree of charge transfer from Cu(I) to O_2. The high quality of the Hammett correlation in Figure 8 also indicates that the oxygenation of the series of *p*-X-C_6H_4-CN adducts constitutes a mechanistically homogeneous reaction series, supporting the assumption that the same mechanism (Scheme 1) applies to all of the L^1Cu(RCN) complexes studied.

Table 4. Relative Free Energies (kJ mol^{-1}) Calculated for the 1:1 Cu−O_2 Adducts, L^1CuO_2 (Within Each Column, Energies Are Relative to the Side-On Singlet)

	gas phase 298 K	gas phase 223 K	THF 298 K	THF 223 K
end-on singlet	16.9	18.3	18.0	19.8
end-on triplet	48.4	51.8	56.8	61.5
side-on singlet	0.0	0.0	0.0	0.0
side-on triplet	22.7	24.0	26.5	28.8

Theoretical Calculations. (A) Structure of the 1:1 Cu−O_2 Adducts. Both side-on (η^2) and end-on (η^1) 1:1 Cu−O_2 adducts supported by L^1 were considered in calculations using DFT and multireference second-order perturbation theory (CASPT2), with either singlet or triplet multiplicities (Experimental Section). Comparing the energies of these adducts (Table 4) indicates that their relative stabilities are affected only minimally by the temperature difference or the use of THF as solvent. Under all conditions, the side-on adducts of a given multiplicity are lower in energy than their end-on counterparts, and of the side-on adducts, the singlet is most stable. These results, as well as key computed properties of the side-on singlet structure for L^1CuO_2, agree well with the experimental findings and differ only slightly from previously reported calculations on L^2CuO_2 (Table S1).[31,32] As discussed more fully below, the O−O bond distance and ν(O−O) values, in conjunction with the degree of multideterminantal character in the CASPT2 wave function and the XAS results, suggest significant Cu(III)−peroxo character for the singlet side-on adduct.

(B) Oxygenation Pathway A. Pathways A and B (Scheme 1), postulated on the basis of the kinetics results, were considered as starting points for theoretical assessment of the mechanism of formation of L^1CuO_2. Turning first to pathway A, we considered the possibility of a rapid pre-equilibrium dissociation of MeCN from L^1CuO_2 to yield "L^1Cu" prior to the rate-controlling O_2-binding event, which could result in either an end-on (η^1) or a side-on (η^2) adduct. The η^1 adduct, if formed, could then isomerize to the final η^2 species. Although inconsistent with the observed kinetics,[65] such a mechanism was analyzed by theory for comparative purposes. Combining the reaction coordinates calculated for the individual steps, we obtain the reaction profile shown in Figure S7 in the Supporting Information. The initial activation barrier corresponds to the loss of MeCN from L^1Cu(MeCN). This step is rate-determining in both the gas phase (298 K, $\Delta G^{\ddagger} = 91.1$ kJ mol^{-1})[66] and in THF solution (223 K, $\Delta G^{\ddagger} = 79.2$ kJ mol^{-1}). In addition to yielding a first-order rate law inconsistent with the bimolecular kinetics observed, the free energy of activation is computed to be higher than that calculated for an associative bimolecular mechanism (see below). The findings thus confirm that a pathway involving prior dissociation of MeCN to yield a "L^1Cu" intermediate is untenable.

(65) The rate law for such a mechanism exhibits an inverse order in [MeCN], which was not observed: $\partial[L^1CuO_2]/\partial t = k_2K_{eq}[L^1Cu(MeCN)][O_2]/[MeCN]$, where the rapid pre-equilibrium $K_{eq} = k_1/k_{-1} = [L^1Cu(MeCN)]/[MeCN]$["$L^1$Cu"] and k_2 refers to the rate-determining oxygenation step.

(66) Unless otherwise indicated, enthalpies, entropies, and free energies pertain to 298 K and gas-phase values.

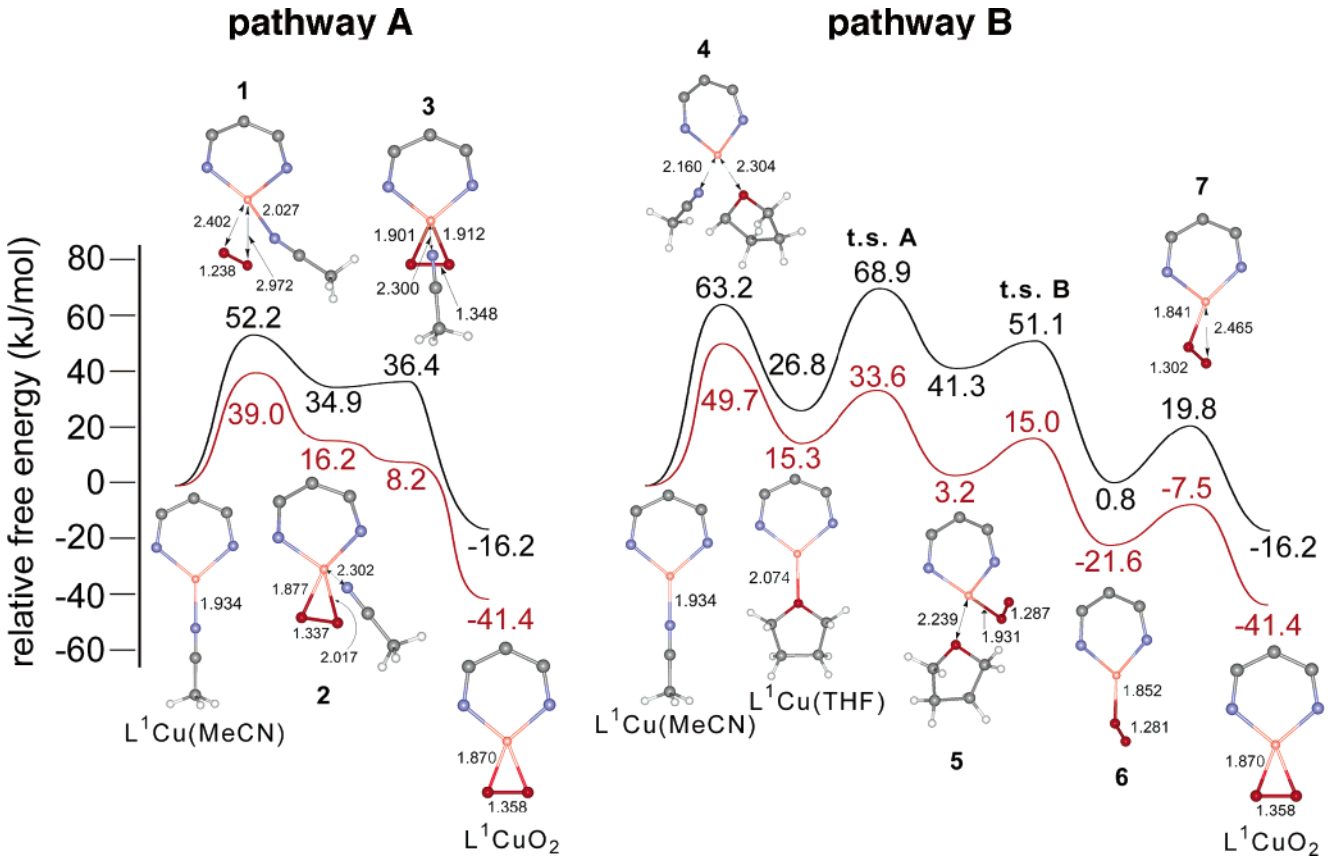

Figure 9. Calculated reaction energy profiles (black line, 298 K, gas phase; red line, 223 K, THF) for (left) the associative bimolecular oxygenation mechanism corresponding to pathway A (Scheme 1) and for (right) the solvolytic oxygenation mechanism corresponding to pathway B (Scheme 1). Cores of the minimized structures are shown, with the substituents on L^1 omitted for clarity and selected interatomic distances indicated (Å). The colors are gray for C, blue for N, red for O, white for H, and pink for Cu. Full details on the protocol used to compute relative energies for all stationary points are provided in the Supporting Information.

A second possibility corresponding to pathway A is an associative mechanism that involves direct binding of O_2 to $L^1Cu(MeCN)$ (Figure 9a). The reaction begins along the triplet surface at long Cu−O_2 distances (Figure S8 and Table S6 in the Supporting Information). The rate-determining transition state (**1**) occurs on the triplet surface at Cu−O1/O2[67] distances of 2.40/2.97 Å (Cu−O_2-midpoint distance of 2.62 Å) and resembles a weak end-on coordination of dioxygen to the Cu center. At this relatively early transition state, the O−O bond length has increased by only 0.023 Å versus that in free dioxygen. The gas-phase activation free energy is 52.2 kJ mol^{-1}, with entropy loss due to O_2 binding being a large contributor (Table 5). Crossing from the triplet to singlet surfaces then occurs at Cu−O1/O2 distances of 2.27/2.52 Å (Cu−O_2-midpoint distance of 2.36 Å), after which an unstable $L^1Cu(MeCN)(O_2)$ intermediate (**2**) is formed. The reaction taking **1** to **2** involves formation of the Cu−O1 bond, with concomitant rotation of O2 toward the Cu center to yield an asymmetric, side-on-bound O_2 moiety in **2**. The MeCN ligand is also only weakly bound at this point, with the Cu−MeCN distance 0.37 Å longer than that in $L^1Cu(MeCN)$. From the $L^1Cu(MeCN)(O_2)$ intermediate (**2**), MeCN is lost in a low-barrier process. At the transition state (**3**), O2 has completed its rotation toward Cu and adopted a position symmetric with respect to O1. The overall reaction is exergonic as expected.

(67) O1 and O2 refer to the oxygen atoms of the O_2 moiety closer to and farther from the Cu center, respectively.

Table 5. Calculated Relative Enthalpies, Entropies, and Free Energies for Species along the Associative Bimolecular Pathway A[a]

species[b]	ΔH^c	ΔS^d	ΔG^c	ΔG^c	ΔG^c	ΔG^c
		298 K[e]		223 K[e]	298 K, THF	223 K, THF
$L^1Cu(MeCN)$	0.0	0.0	0.0	0.0	0.0	0.0
1	10.1	−141.5	52.2	41.6	49.1	39.0
2	−13.4	−161.9	34.9	22.8	28.2	16.2
3	−11.4	−160.6	36.4	24.4	20.7	8.2
L^1CuO_2	−22.9	−22.8	−16.2	−17.7	−37.3	−41.4

[a] Details pertaining to the calculation of these quantities can be found in Table S5 in the Supporting Information. [b] Gas phase. [c] Units are in kJ mol^{-1}. [d] Units are in J K^{-1} mol^{-1}. [e] All energy comparisons are for stoichiometrically equivalent species.

Smaller activation barriers and smaller free energy changes for individual reaction segments were calculated at 223 K compared to 298 K, due to the decreased influence of the entropy changes on the free energy values (Table 5). When solvation by THF was included in the calculations, **1** remains the rate-determining transition-state structure, but **2**, which is an intermediate in the gas phase at 298 K by virtue of being marginally lower in energy than **3**, is apparently no longer a stationary point. In addition, due to the large solvation energy for MeCN in THF (approximately −29 kJ mol^{-1}), the overall reaction becomes more exergonic when solvent effects are included (as reflected by the significantly decreased energy of L^1CuO_2, Table 5). Notably, the activation parameters calculated

for the bimolecular pathway A in THF ($\Delta H^{\ddagger} = 14.9$ kJ mol^{-1}, $\Delta S^{\ddagger} = -108.0$ J K^{-1} mol^{-1}) are in excellent agreement with those measured experimentally ($\Delta H^{\ddagger} = 18$ kJ mol^{-1}, $\Delta S^{\ddagger} = -100$ J K^{-1} mol^{-1}; see Tables 2 and S7).

The flow of electrons as the pathway in Figure 9a is traversed may be assessed by considering simple Mulliken charge distributions for the O and Cu atoms, as well as L^1 and MeCN, calculated at 223 K in THF (Table S8 in the Supporting Information). In the reactant $L^1Cu(MeCN)$, the positive charge on Cu is balanced by the negatively charged L^1. At the transition state **1**, the O_2 fragment begins to accept electron density from Cu into its π^* orbitals, but L^1 stabilizes the oxidized Cu center, giving a net effect of electron density flowing from L^1 to the O_2 moiety and minimal change in the charge on Cu (0.02 units). The degree of electron transfer to the O_2 unit in **1** is 20% relative to the product L^1CuO_2, according to a comparison of the total Mulliken charges for the O atoms. Upon formation of **2**, the reduction of O_2 is nearly complete, with the additional electron density on the O atoms having come in almost equal amounts from the Cu center (now ~50% oxidized) and L^1. Release of MeCN from **2** to give L^1CuO_2 results in the last significant oxidation of the L^1Cu moiety, with the increases in the Mulliken charges of L^1 and Cu again being nearly equal. Comparing $L^1Cu(MeCN)$ to L^1CuO_2, the overall process of O_2 reduction involves transfer of electron density to the dioxygen fragment in nearly equal amounts from both the Cu and the β-diketiminate ligand. Note that we do not suggest that there is any equality between a computed Mulliken charge and a formally assigned metal oxidation state; rather, our analysis here is simply to provide insight into how electronic charge is internally distributed along the reaction path, particularly insofar as that redistribution is expected to influence the Hammett plot for substituted nitrile ligands.

(C) Oxygenation Pathway B. The solvolytic pathway B (Scheme 1) may be divided into two segments; first, the exchange of MeCN in $L^1Cu(MeCN)$ for THF to yield $L^1Cu(THF)$, and second, the reaction of dioxygen with $L^1Cu(THF)$ to give L^1CuO_2. As already noted above, a purely dissociative process that involves loss of MeCN to yield the intermediate "L^1Cu" that would then be trapped by THF has an activation energy too high to be considered to be reasonable (Figures S7 and S9 in the Supporting Information). An energetically more favorable alternative is a concerted interchange mechanism (Figure 9b) involving a transition-state structure **4** with MeCN and THF both weakly bound. The reaction is endergonic, $\Delta G = +26.8$ kJ mol^{-1} (Table 6), consistent with the relative strengths of MeCN and THF coordination to Cu(I) (MeCN > THF).

As in the calculations for oxygenation of $L^1Cu(MeCN)$ via pathway A, a mechanism for reaction of $L^1Cu(THF)$ with O_2 involving prior dissociation of THF and trapping of the resultant "L^1Cu" species by O_2 has an activation free energy (from $L^1Cu(THF)$) that is greater than an associative alternative by 25.6 kJ mol^{-1} (Figures 9b and S9). The latter, kinetically preferred route involves the formation of an unstable intermediate $L^1Cu(THF)(O_2)$ (**5**), in which O_2 is bound end-on to Cu, via **t.s. A**. Note that the end-on coordination of O_2 in **5** contrasts with the side-on binding in its counterpart in the associative pathway A, compound **2**. This difference may be attributed to the greater steric bulk of THF compared to that of MeCN. At long Cu−O1 distances during the process by which $L^1Cu(THF)$ converts to **5**, the reaction takes place along the triplet surface. Crossover to the singlet surface occurs at a Cu−O1 distance of 2.46 Å, thereafter yielding the singlet product **5** in which the O_2 fragment has an O−O distance 0.072 Å longer than that in dioxygen. Loss of THF from **5** yields an end-on Cu−O_2 adduct (**6**), which then isomerizes to the final product L^1CuO_2. At the early transition state (**7**) for this reaction, the O−O bond length increases by a minimal 0.021 Å. The product L^1CuO_2 is formed as O2 rotates closer to Cu to give symmetric side-on binding of dioxygen to Cu, and the O−O bond length grows by another 0.056 Å as the reduction of O_2 is completed.

Table 6. Calculated Relative Enthalpies, Entropies, and Free Energies for Species along the Solvolytic Pathway B[a]

species[b]	ΔH^c	ΔS^d	ΔG^c	ΔG^c	ΔG^c	ΔG^c
		298 K[e]		223 K[e]	298 K, THF	223 K, THF
$L^1Cu(MeCN)$	0.0	0.0	0.0	0.0	0.0	0.0
4	15.9	−158.9	63.2	51.2	60.6	49.7
$L^1Cu(THF)$	19.0	−26.0	26.8	24.9	18.1	15.3
t.s. A	19.0	−164.8	68.9	59.3	46.5	33.6
5	−7.8	−164.8	41.3	28.9	16.1	3.2
t.s. B	2.0	−164.8	51.1	38.7	16.9	15.0
6	−0.2	−3.4	0.8	0.6	−19.3	−21.6
7	14.1	−19.4	19.8	18.5	0.1	−7.5
L^1CuO_2	−22.9	−22.8	−16.2	−17.7	−37.3	−41.4

[a] Details pertaining to the calculation of these quantities can be found in Table S5 in the Supporting Information. [b] All energy comparisons are for stoichiometrically equivalent species. [c] Units are in kJ mol^{-1}. [d] Units are in J K^{-1} mol^{-1}. [e] Gas phase.

The effects of changing temperature from 298 to 223 K and from being in the gas phase to in THF solvent are significant along the solvolytic pathway. The most important consequence of these temperature and solvent effects is a change in the rate-determining transition state from **t.s. A** at 298 K in the gas phase to **4** at 223 K in THF. That is, binding of dioxygen to $L^1Cu(THF)$ is rate-determining in the gas phase at the higher temperature, whereas the exchange of THF for MeCN becomes rate-determining in solution at the lower temperature, in agreement with the experimental conclusions. In addition, the activation parameters calculated for pathway B in THF ($L^1Cu(MeCN) \rightarrow L^1Cu(THF)$, $\Delta H^{\ddagger} = 27.2$ kJ mol^{-1}, $\Delta S^{\ddagger} = -100.1$ J K^{-1} mol^{-1}) are almost identical to those measured experimentally ($\Delta H^{\ddagger} = 30$ kJ mol^{-1}, $\Delta S^{\ddagger} = -98$ J K^{-1} mol^{-1}, Tables 2 and S7).

These results including solvation and lowering the temperature may be traced to several effects. As in the bimolecular pathway A, smaller contributions from entropy changes at the lower temperature are reflected in the ΔG values. Solvent effects are also noticeable in reaction steps involving the binding or release of THF (solvation energy of approximately −10.5 kJ mol^{-1}) or MeCN, both of which, in contrast to dioxygen, are well solvated in THF. In addition, entropic considerations tied to the explicit role that THF solvent molecules play in reactions along the solvolytic pathway contribute to lower ΔG values for species incorporating THF (see Table S7).

Of these three effects, only the desolvation of THF leads to a destabilization of transition state **4** versus $L^1Cu(MeCN)$ at 223 K in THF compared to 298 K in the gas phase. Inclusion of the two entropic effects more than overcomes the desolvation penalty, yielding an activation energy for solvolysis which is 13.5 kJ mol^{-1} lower than that at 298 K in the gas phase (Table

6). In contrast, the energy of **t.s. A** (which, to be stoichiometrically equivalent to the reactants, i.e., $L^1Cu(MeCN)$, O_2, and THF, includes the energy of MeCN) is lowered by 35.3 kJ mol^{-1} in solution at the lower temperature. The effect of the negative $\Delta S^{\ddagger}$ upon $\Delta G^{\ddagger}$ is decreased by ~8.5−12.5 kJ mol^{-1}, while binding of solvent THF in **t.s. A** lowers $\Delta G^{\ddagger}$ by ~6.3 kJ mol^{-1}. Moreover, the exchange of solvent-derived ligands in going from $L^1Cu(MeCN)$ to $L^1Cu(THF)$, leading to the release of the more favorably solvated MeCN into solution, leads to an overall lower solvation energy for **t.s. A** compared to that for $L^1Cu(MeCN)$. The energy of **t.s. B** is also analogously lowest at 223 K in THF. The inclusion of solvation energy for both MeCN and THF at points **6**, **7**, and product L^1CuO_2 accounts for their noticeably lower total free energies in THF as opposed to those in the gas phase. The result of all of these effects is a change in the rate-determining step, from dioxygen coordination to $L^1Cu(THF)$ in the gas phase at the higher temperature to exchange of THF for MeCN in solution at the lower temperature, as found by experiment.

Mulliken charge distributions for the species involved in the solvolytic pathway B (Figure 9b) are listed in Table S8 (Supporting Information). In this pathway, the process of dioxygen activation begins with the formation of **5** from $L^1Cu(THF)$ and O_2. Similar to the results for the bimolecular pathway, the negative charge borne by the O_2 moiety in **5** originates in nearly equal amounts from both Cu and the ligand L^1, with the oxidation of Cu ~50% complete and the reduction of dioxygen about two-thirds complete relative to the final product L^1CuO_2. As THF, which bears a partial positive total Mulliken charge in **5**, is lost to give **6**, the charge assignable to the ligand L^1 decreases further while the Cu is oxidized only minimally. This can be explained through simultaneous oxidation of Cu and donation of electron density from the still relatively electron-rich ligand L^1 to Cu to create the net effect of a decreased Mulliken charge on L^1. Notably, at **6**, the charge on the ligand is nearly equal to its final value in the product L^1CuO_2, indicating that further charge donation from the ligand to Cu and/or O_2 does not occur beyond this point. Conversion from the end-on to side-on 1:1 Cu−O_2 adduct brings about the remaining oxidation and reduction of Cu and O_2, respectively, as the O_2 group becomes more strongly bound to the Cu center.

Discussion

Structure of 1:1 Cu−O_2 Adducts. The better quality X-ray crystallographic data for L^2CuO_2 in conjunction with the Cu K-edge XAS and EXAFS data on L^1CuO_2 provide important corroboration for the previously proposed electronic structure for these side-on (η^2) 1:1 Cu−O_2 adducts.[31,32,42] Although disorder problems continue to complicate the X-ray crystallographic analysis and mitigate the significance of the observed interatomic distances, the new data yield an O−O distance of 1.392(12) Å that is significantly shorter than that determined previously (1.44 Å) and in much closer agreement to that of a theoretical prediction (1.376 Å)[31] made at a level of theory that has already been used to correct another inaccurately reported O−O bond length in a side-on metal−dioxygen complex crystal structure.[32] This revised distance brings the complex more in line with a trend noted previously in a plot of O−O vibrational frequency versus O−O bond distance for η^2 1:1 metal−O_2 adducts.[32] In this plot, L^2CuO_2 lies in the center of a continuum between metal−peroxide and −superoxide complexes,[68] suggesting that it has a novel electronic structure insofar as it has significant Cu(III)−peroxide character.

To further assess this notion experimentally, Cu K-edge XAS data were acquired and interpreted within the context of a previous study,[62] in which it was demonstrated that the pre-edge 1s → 3d transition energy may be used as a diagnostic tool for distinguishing Cu(II) and Cu(III) oxidation states. The pre-edge position is affected by two factors, the ligand field strength and the effective nuclear charge (Z_{eff}) on the metal. An increase in the oxidation state (Z_{eff}) causes a shift of the 1s core orbital to deeper binding energy and a larger repulsive interaction between the $d_{x^2-y^2}$ orbital (LUMO for Cu(III)) and the ligand donor orbitals, inducing a shift of the LUMO to higher energy. As a result, the 1s → 3d energy difference becomes larger, which is manifested in the pre-edge shifting to higher energies for Cu(III) compared to Cu(II). The observed congruence between the energy and intensity of the pre-edge feature for L^1CuO_2 and a bis(μ-oxo)dicopper(III,III) complex attests to similar oxidation levels for the metal ions in these complexes and supports attribution of significant Cu(III) character to L^1CuO_2. Nonetheless, there are differences between the XAS spectra for these compounds, in particular, in the energies and intensities of the two-electron 1s → 4 p + LMCT shakedown transitions. The 1s → 4p + LMCT shakedown transition at ~8987 eV is less intense in L^1CuO_2 relative to that of the bis(μ-oxo) species, which indicates a more covalent interaction in the bis(μ-oxo) compared to that in the side-on peroxo L^1CuO_2 system. This is consistent with the differences in ligand-to-metal charge-transfer (LMCT) intensity between the complexes in absorption spectra, where the bis(μ-oxo) features have an intensity an order of magnitude higher than those of L^1CuO_2. This difference in peroxo− relative to oxo−Cu covalency reflects differences both in the energies and the natures of the valence orbitals of peroxide and oxide and the strong donor interaction of the β-diketiminate ligand with the Cu center, which impacts the peroxide−Cu bond. Also, both of the 1s → 4p + LMCT shakedown and pre-edge transitions are to slightly lower energy in L^1CuO_2, which indicates a slightly lower Z_{eff} on Cu, again reflecting the high donor strength of the β-diketiminate.

The Cu−O/N bond distances from the X-ray crystallographic and EXAFS data also support significant Cu(III) character in the $LCuO_2$ complexes. To draw this conclusion, we compared the crystallographically determined distances between Cu and the N atoms of β-diketiminate ligands for 36 reported complexes (Table S9 in the Supporting Information); other metal−ligand bond distances were ignored due to complicating differences in ligand donor atom types.[69] The results are summarized in Table 7, wherein the compounds are grouped according to coordination number and Cu oxidation state. When the average Cu−N distances for each group are compared, caveats are the considerable overlap in the ranges of Cu−N distances between the groups (also reflected in the standard deviations) and the small data set for Cu(III) that is restricted to two bis(μ-oxo)-dicopper structures. Nonetheless, and as expected, at parity of coordination number, an increase in oxidation level is ac-

(68) The validity of this continuum has been questioned recently, but in more recent work, the arguments presented in this critique have been refuted (ref 42): Pantazis, D. A.; McGrady, J. E. *Inorg. Chem.* **2003**, *42*, 7734.

Table 7. Summary of Cu−N(β-Diketiminate) Distance Data from Available X-ray Crystal Structures (Full List Provided in Table S9 in the Supporting Information)

coordination number	oxidation state	average[a]	range[a]	standard deviation[a]	entries[b]
3	I	1.940	1.90−1.992	0.025	26
3	II	1.887	1.858−1.923	0.020	18
4	II	1.926	1.88−1.987	0.021	30
4	III	1.892	1.881−1.902	0.009	4

[a] Units are in Å. [b] Number of independent Cu−N(β-diketiminate) distances considered.

companied by a decrease in the average Cu−N distance. The near identity of the average Cu−N distances for three-coordinate Cu(II) and four-coordinate Cu(III) reflect the importance of coordination number in the overall analysis. Notably, the Cu−N distances in L^2CuO_2 (1.856(6) Å) and L^1CuO_2 (avg Cu−N/O = 1.83 Å) are less than any of the average values listed in Table 7. Moreover, while closely congruent with the shortest reported distance for a three-coordinate Cu(II) complex (1.858(2) Å), the distances for the 1:1 adducts are less than any of those reported for four-coordinate compounds at Cu(II) or Cu(III) levels. Taken together, the data are consistent with a formulation for $LCuO_2$ that features considerable Cu(III)−peroxo character.

It is of interest to compare the bonding description for $LCuO_2$ and that for the related complex $[PhTt^{Ad}]NiO_2$ reported recently ($PhTt^{Ad}$ = phenyltris((1-adamantylthio)methyl)borate).[70] The Ni adduct was assigned as a side-on (η^2) O_2 complex on the basis of EXAFS spectroscopy and density functional calculations. The authors concluded that a Ni(II)−superoxo formalism is most consistent with (a) its XAS edge energy ∼1 eV below that of a bis(μ-oxo)dinickel(III,III) complex, (b) its EPR spectrum, which contains a signal indicative of a single unpaired electron highly localized in a Ni d_{z^2} orbital, and (c) a calculated O−O distance of 1.38 Å. In addition, DFT calculations showed that the SOMO is indeed highly localized on Ni, and that the doubly occupied HOMO below the SOMO covalently mixes the Ni $d_{x^2-y^2}$ orbital with the in-plane O_2 π^*. The authors interpret this doubly occupied orbital to represent a strong antiferromagnetic coupling between a superoxide-like O_2 and Ni(II).

Our own analysis of this situation suggests that the Ni−O_2 interaction is somewhat analogous to that which we have defined for $LCuO_2$ and should be thought of as lying roughly midway along a continuum between Ni(II)−superoxide and Ni(III)−peroxide character,[32] where the connection between the two is dictated by the degree of charge transfer from Ni to O_2 in the covalent orbital in question. The published computational results support this analysis from a structural standpoint.[70] Thus, the computed O−O bond length of 1.38 Å is shorter than those typically found in peroxides (ca. 1.42 Å or greater) but is substantially longer than a typical superoxide bond length, in particular the 1.29 Å distance computed by the authors for an isomer of $[PhTt^{Ad}]NiO_2$, in which the O_2 fragment is bound end-on to Ni and is much more accurately described as a pure Ni(II)−superoxide species. Finally, we note that while there appear to be gross similarities between the bonding descriptions for the Cu and Ni species, differences in placement along the superoxo−peroxo continuum are likely, particularly in view of the differences between the complex geometries and the electron-donating capabilities of their supporting ligands.

Mechanism of Formation of L^1CuO_2. The data acquired from cryogenic stopped-flow kinetic experiments for the oxygenation of $L^1Cu(NCR)$ complexes support a mechanism (Scheme 1) involving two paths that differ kinetically with respect to the order in O_2 (eq 8). According to this mechanism, direct bimolecular attack of O_2 onto the Cu(I) complex (pathway A, first-order dependence on O_2) occurs in parallel with reversible replacement of nitrile by THF followed by oxygenation (pathway B, no dependence on O_2). Precedence for this model is amply provided by numerous studies of ligand-substitution processes in square planar d^8 complexes that proceed by dual paths, one that is dependent on incoming ligand and the other involving a solvent-assisted process that is not.[64] Solvent interference in oxygenations of Cu(I) complexes also has been reported, wherein the reactions are retarded in the presence of free nitrile.[27,71−73] Similarly, in the presence of excess MeCN (or other nitriles), the reaction of $L^1Cu(MeCN)$ with O_2 is slowed. Under these conditions, pathway B is effectively shut down, enabling detailed assessment of the direct bimolecular pathway A.

Activation parameters obtained for pathway A for the oxygenation of $L^1Cu(MeCN)$ are compared to illustrative values reported previously for analogous O_2-dependent reactions of other mononuclear Cu(I) complexes, as shown in Table 2.[22b,27,28,74] The low activation enthalpy observed for $L^1Cu(MeCN)$ is similar to that observed for other compounds, but the $\Delta S^{\ddagger}$ value sets a record low for such reactions. We suggest that this highly unfavorable (negative) entropy of activation is due to the high degree of steric hindrance around the metal ion created by L^1. This hypothesis is supported by previous work that established a connection between $\Delta S^{\ddagger}$ and metal complex steric properties in oxygenation reactions.[72,75,76]

Further insight into pathway A for the reaction of $L^1Cu(MeCN)$ with O_2 was provided by a Hammett study of oxygenations performed in the presence of excess quantities of various *para*-substituted benzonitriles. The excellent correlation of k_A with substituent σ_p values (Figure 8) represents a quantitative measure of the sensitivity of oxygenation rate constants to electronic effects across a mechanistically homogeneous series of metal complexes. The resulting ρ of −0.34 reflects a modest build-up of positive charge at the metal center in the rate-controlling transition state or, in other words, nucleophilic character for the metal complex in the oxygenation process. This result is not surprising considering the degree of reduction of the O_2 molecule and corresponding degree of oxidation of the L^1Cu fragment in the L^1CuO_2 product, shown above to have considerable Cu(III)−peroxide character. A

(69) We considered an alternative bond valence sum analysis but chose the present simpler method due to complications associated with an appropriate choice of reference (r_0) values: (a) Brown, I. D.; Altermatt, D. *Acta Crystallogr.* **1985**, *B41*, 240 and 244. (b) Thorp, H. H. *Inorg. Chem.* **1992**, *31*, 1585. (c) Hati, S.; Datta, D. *J. Chem. Soc., Dalton Trans.* **1995**, 1177. (d) Liu, W.; Thorp, H. H. *Inorg. Chem.* **1993**, *32*, 4102.

(70) Fujita, K.; Schenker, R.; Gu, W.; Brunold, T. C.; Cramer, S. P.; Riordan, C. G. *Inorg. Chem.* **2004**, *43*, 3324.

(71) Becker, M.; Schindler, S.; van Eldik, R. *Inorg. Chem.* **1994**, *33*, 5370.

(72) Karlin, K. D.; Kaderli, S.; Zuberbühler, A. D. *Acc. Chem. Res.* **1997**, *30*, 1399.

(73) Liang, H.-C.; Karlin, K. D.; Dyson, R.; Kaderli, S.; Jung, B.; Zuberbühler, A. D. *Inorg. Chem.* **2000**, *39*, 5884.

(74) Halfen, J. A.; Mahapatra, S.; Wilkinson, E. C.; Kaderli, S.; Young, V. G., Jr.; Que, L., Jr.; Zuberbühler, A. D.; Tolman, W. B. *Science* **1996**, *271*, 1397.

(75) Rybak-Akimova, E. V.; Marek, K.; Masarwa, M.; Busch, D. H. *Inorg. Chim. Acta* **1998**, *270*, 151.

(76) Kryatov, S. V.; Rybak-Akimova, E. V.; MacMurdo, V. L.; Que, L., Jr. *Inorg. Chem.* **2001**, *40*, 2220.

similar trend of greater O_2 reactivity with increased ligand electron donation was reported previously for some other Cu(I) complexes,[27,72,77,78] but quantitative Hammett-type correlations between O_2 reactivity and substituent electronic properties have only been drawn in one instance.[79] In this study of the oxygenation of Cu(I) complexes of substituted phenanthrolines in which O_2 adducts were not isolated, a plot of the third-order rate constants (rate = k[Cu(I)]^2[O_2]) yielded $\rho = -0.71$. Thermodynamic stabilization of O_2 binding to metal sites by electron-donating ligands has been demonstrated for numerous systems (e.g., hemes and analogues),[80] but this effect has been attributed primarily to decreased rate constants for O_2 dissociation, with little contribution from changes in rate constants for the O_2 association step.[75,81,82]

Theoretical calculations corroborate the mechanistic picture deduced from the experimental results and reveal further details of the reaction trajectory for pathway A. Importantly, excellent agreement between experimentally and theoretically determined activation parameters for the oxygenation of L^1Cu(MeCN) via pathway A when THF solvation is appropriately considered lends support to the calculated reaction profile. According to these calculations, the transition state (**1**) features an O_2 fragment that is weakly bound and an MeCN that is significantly displaced, yet still strongly bound; this is consistent with the observed Hammett rate constant correlation when substituted benzonitriles were used. The calculations also showed that loss of MeCN from **1** and movement of the coordinated O_2 moiety to its final symmetric η^2 position is strongly exergonic, in agreement with the observed irreversibility of the oxygenation reaction. Such irreversibility is unique among Cu(I)−O_2 reactions and, in combination with the absence of dicopper complex formation for this system that is more typical in Cu(I)−O_2 chemistry,[17] enables the use of the L^1CuO_2 as a synthon for the construction of novel asymmetric bimetallic[31] and heterobimetallic complexes.[83]

The measured activation parameters for pathway B (Table 2) reflect the process by which THF substitutes for coordinated MeCN (k_B, k_{B1}) since this step is slow and rate-controlling relative to the subsequent oxygenation of L^1Cu(THF). It is probably coincidental that the entropy of activation for the ligand substitution step in pathway B is identical within experimental error to that measured for the oxygenation step of pathway A. Nonetheless, one may argue that steric hindrance for addition of a ligand (THF or O_2) to L^1Cu(MeCN) underlies the large negative values found for both steps, particularly in view of the mechanistic similarities between them (associative processes; compare **1** to **4** in Figure 9). In contrast, the value of $\Delta H^{\ddagger}$ is significantly larger for the addition of THF (30 kJ mol^{-1}) than for the addition of O_2 (18 kJ mol^{-1}) to L^1Cu(MeCN). This difference may be rationalized by considering that the nascent Cu−O_2 bond(s) are stronger than the nascent Cu−THF interaction. The weak Cu(I)−THF bond also is reflected in the endergonic nature of the conversion of L^1Cu(MeCN) to L^1Cu(THF) ($\Delta G = 15.3$ kJ mol^{-1} at 223 K in THF; Table 6).

In addition, the weak Cu(I)−THF interaction contributes to the lower barrier for oxygenation of L^1Cu(THF) relative to that of L^1Cu(MeCN), as reflected by the calculated (223 K, THF) free energy differences between L^1Cu(MeCN) and **1** (39.0 kJ mol^{-1}) versus between L^1Cu(THF) and **t.s. A** (18.3 kJ mol^{-1}). The reaction trajectories for these oxygenations differ as well, such that O_2 adopts a side-on position essentially directly upon binding to the copper ion in pathway A (without an end-on intermediate) but first binds end-on in its reaction with L^1Cu(THF) prior to rapid isomerization to its final side-on position in L^1CuO_2 in pathway B (Figure 9). We postulate that this difference derives from steric factors; direct side-on binding of O_2 is inhibited by the greater bulk of THF relative to MeCN. Our finding of greater oxygenation reactivity for L^1Cu(THF) compared to that for L^1Cu(MeCN) is consistent with previous reports for the (TMPA)Cu(I) system, where (a) oxygenation of (TMPA)Cu(MeCN) in EtCN was slower than in THF and (b) (TMPA)Cu(THF) generated by photolysis of (TMPA)-$CuCO^+$ in THF reacted with O_2 at a rate close to the diffusion limit.[27]

Analysis of the Mulliken charge changes, which take place in the course of the reaction (Table S8), reveals that the electron density responsible for the reduction of dioxygen originates not entirely (or even largely) from the Cu(I) center. Rather, the Cu(I) center and the formally negatively charged β-diketiminate ligand contribute equally to the reduction of dioxygen. The electron-rich ligand thus plays a central role not only in stabilizing the oxidized Cu center but also in allowing for efficient reduction of the O_2 moiety. The importance of the ligand is especially noticeable in the transition state (**1**) in the bimolecular pathway, in which charge essentially flows from the β-diketiminate group, through the Cu, and into dioxygen. Notably, the electronics at this transition state, in which the L^1Cu unit has become partially oxidized, are consistent with the negative Hammett ρ value, implicating positive charge build-up on LCu at the transition state of the bimolecular pathway. Finally, one may also draw a conceptual connection between the metal−ligand interactions during O_2 binding by LCu to those postulated during dioxygen activation by heme−iron centers, wherein the metal has been suggested to "relay the electron flux" from the porphyrin to a bound dioxygen moiety.[84]

Conclusion

Detailed insight into the process of O_2 activation at a single copper center supported by β-diketiminate ligands has been obtained through a synergistic combination of experiment and theory. The degree of O_2 reduction upon binding to the LCu system is extensive, as indicated by previous theoretical calculations and vibrational data,[30−32] as well as the new X-ray crystallographic, Cu K-edge XAS, EXAFS, and theoretical results reported herein, all of which are consistent with significant Cu(III)−peroxo character in $LCuO_2$. A dual pathway

(77) Karlin, K. D.; Nasir, M. S.; Cohen, B. I.; Cruse, R. W.; Kaderli, S.; Zuberbühler, A. D. *J. Am. Chem. Soc.* **1994**, *116*, 1324.
(78) Lee, D.-H.; Wei, N.; Murthy, N. N.; Tyeklar, Z.; Karlin, K. D.; Kaderli, S.; Jung, B.; Zuberbühler, A. D. *J. Am. Chem. Soc.* **1995**, *117*, 12498.
(79) Arce, J. A.; Spodine, E.; Zamudio, W. *J. Inorg. Nucl. Chem.* **1976**, *38*, 2029.
(80) Momenteau, M.; Reed, C. A. *Chem. Rev.* **1994**, *94*, 659.
(81) Momenteau, M.; Loock, B.; Lavalette, D.; Tétreau, C.; Mispelter, J. *J. Chem. Soc., Chem. Commun.* **1983**, 962. (b) Traylor, T. G.; Traylor, P. S. *Annu. Rev. Biophys. Bioeng.* **1982**, *11*, 105.
(82) Collman, J. P.; Brauman, J. I.; Doxsee, K. M.; Sessler, J. L.; Morris, R. M.; Gibson, Q. H. *Inorg. Chem.* **1983**, *22*, 1427.
(83) Aboelella, N. W.; York, J. T.; Reynolds, A. M.; Fujita, K.; Kinsinger, C. R.; Cramer, C. J.; Riordan, C. G.; Tolman, W. B. *Chem. Commun.* **2004**, 1716.
(84) (a) Silaghi-Dumitrescu, R. *J. Biol. Inorg. Chem.* **2004**, *9*, 471. (b) Johansson, M. P.; Blomberg, M. R. A.; Sundholm, D.; Wikström, M. *Biochim. Biophys. Acta* **2003**, *1553*, 183.

mechanism for the oxygenation of $L^1Cu(RCN)$ in THF and THF/RCN mixtures is proposed on the basis of cryogenic stopped-flow kinetics data and theoretical calculations. One pathway (B in Scheme 1) involves rate-controlling solvolysis via an associative interchange mechanism, followed by rapid substitution of the weakly bound THF ligand by O_2. Calculations indicate that in this path, end-on O_2 coordination occurs prior to rapid isomerization to the final side-on structure of the product. In the presence of excess RCN, this solvolytic pathway is suppressed and a direct bimolecular, associative substitution by O_2 occurs instead (pathway A). A detailed picture of this oxygenation process has been provided by the experimental kinetic data, in particular the $\Delta H^{\ddagger}$, $\Delta S^{\ddagger}$, and Hammett ρ values, in conjunction with a theoretical assessment of the reaction trajectory (both in the gas phase and in THF solution) that yielded activation parameters highly congruent with those obtained by experiment. The results suggest that electron density flows from both the β-diketiminate and the Cu ion to the O_2 moiety, with a transition-state structure that features both coordinated nitrile and dioxygen (weakly bound, in asymmetric fashion). Taken together, the results of this study yield a comprehensive understanding of O_2 binding in a synthetic copper system, a fundamentally important process that represents a model for how dioxygen activation may occur at single copper centers in biology and catalysis.

Acknowledgment. We thank the NIH (GM47365 to W.B.T., postdoctoral fellowship to B.F.G., DK-31450 to E.I.S., RR-01209 to K.O.H.), NSF (CHE-0203346 to C.J.C., CHE-0111202 to E.V.R.-A., predoctoral fellowship to N.W.A.), and the Research Corporation (RI0223 to E.V.R.-A.). ChemMatCARS Sector 15 is principally supported by the National Science Foundation/Department of Energy under Grant CHE-0087817, and by the Illinois board of higher education. The Advanced Photon Source is supported by the U.S. Department of Energy, Basic Energy Sciences, Office of Science, under Contract W-31-109-Eng-38. The XAS data were measured at SSRL, which is supported by the U.S. Department of Energy, Basic Energy Sciences. The SSRL Structural Molecular Biology Program is supported by the U.S. Department of Energy, Office of Biological and Environmental Research, and by the National Institutes of Health, National Center for Research Resources, and Biomedical Technology Program.

Supporting Information Available: Calculation details, kinetic data, X-ray structure representations, and tabulation of bond distances for β-diketiminate complexes of copper (PDF), and X-ray crystallographic data (CIF). This material is available free of charge via the Internet at http://pubs.acs.org.

JA045678J